`

Trade-off among Mechanical Properties and Energy Consumption in Multi-pass Friction Stir Processing of Al 7075-T651 Alloy Employing Hybrid Approach of Artificial Neural Network and Genetic Algorithm

Shahin Hassanzadeh Bazaz

Submitted to the
Institute of Graduate Studies and Research
in partial fulfillment of the requirements for the Degree of

Master of Science
in
Mechanical Engineering

Eastern Mediterranean University
July 2014
Gazimağusa, North Cyprus

`

Approval of the Institute of Graduate Studies and Research

Prof. Dr. Elvan Yılmaz
Director

I certify that this thesis satisfies the requirements as a thesis for the degree of Master of Science in Mechanical Engineering.

Prof. Dr. Uğur Atikol
Chair, Department of Mechanical Engineering

We certify that we have read this thesis and that in our opinion it is fully adequate in scope and quality as a thesis for the degree of Master of Science in Mechanical Engineering.

Asst. Prof. Dr. Mostafa Ranjbar
Co-supervisor

Asst. Prof. Dr. Ghulam Hussain
Supervisor

Examining Committee

1. Assoc. Prof. Dr. Hasan Hacışevki
2. Asst. Prof. Dr. Ghulam Hussain
3. Asst. Prof. Dr. Neriman Özada
4. Asst. Prof. Dr. Mostafa Ranjbar
5. Dr. Kian Parham

`

ABSTRACT

Friction Stir Processing (FSP) is a solid state and thermomechanical processing technique that modify and improve the microstructural and mechanical properties of the material to achieve better performance in less time, using a simple and inexpensive tool and low production cost. Processed zone contains modified mechanical properties, fine grained, equaled and homogeneous microstructures. Discussions about efficient use of energy and expense have become more frequent in many sectors of industry. During manufacturing processes, power consumption of components and potential for savings can be evaluated and measures can be defined for the efficient use of energy. In the present work, FSP was applied on the Aluminum 7075-T651 alloy sheet. Application of multi-objective multivariable genetic optimization in FSP was presented. A trade-off among various mechanical properties of an aerospace alloy and energy consumed during FSP was sought out. At first, the experimental data regarding the elongation, tensile strength, hardness and the consumed electrical energy with respect to various spindle rotational speed and feed rate of FSP were measured. Then an Artificial Neural Network-based approximation approach was used to approximate the value of measured data during the Genetic Optimization. The properties like elongation, tensile strength and hardness were maximized while the cost of consumed electrical energy was minimized.

Keywords: Friction Stir Processing; Al7075; Multi-objective; Genetic Algorithm; Optimization; Artificial Neural Networks.

`

ÖZ

Sürtünme karıştırma işlemi (FSP) basit ve masrafsız araçlar kullanarak, üretim maliyeti az olan ve kısa sürede daha iyi bir performans elde etmek için kullanılan, maddenin mikroyapısal ve mekanik özelliklerini geliştirmek ve modifiye etmeyi amaçlayan bir katı hal ve termomekanik işlem tekniğidir. İşlenmiş bölge modifiye edilmiş mekanik özellikler, ince taneli, eşitlenmiş ve homojen mikroyapılar içermektedir. Enerji kullanımı ve masraflarla ilgili tartışmalar, endüstrinin birçok sektöründe artmaktadır. Üretim işlemi süresince, elemanların güç tüketimi ve olası enerji tasarrufları değerlendirilebilir ve etkili enerji kullanımı için gerekli ölçüler tanımlanabilir. Bu çalışmada FSP, Al 7075-T651 alaşımlı saca uygulanmıştır. FSP'nin çok amaçlı, çok değişkenli, genel optimizasyonu bu çalışmada sunulmuştur. Hava uzay alaşımındaki çeşitli mekanik özellikler arasındaki dönüşüm ve FSP sırasındaki enerji tüketimi gözlemlenmiştir. Öncelikle, genişleme, çekme direnci, katılık, ilerleme hızı ve dönme hızı bağlamında tüketilen elektrik enerjisi ile ilgili deneysel veriler ölçülmüştür. Daha sonra, genetik optimizasyon sırasında ölçülen verileri uyumlaştırmak amacıyla, yapay sinir ağı temelli uyumlaştırma yaklaşımı kullanılmıştır. Genişleme, çekme dirence ve katılık gibi özellikler artırılırken, tüketilen elektrik enerjisinin maliyeti ise azalmaktadır.

Anathar Kelimeler: Sürtünme Karıştırma İşlemi; Al7075; Çok amaçlı; Genetik Algoritma; Optimizasyon; Yapay Sinir Ağları.

`

TO MY FAMILY

`

ACKNOWLEDGMENT

I would like to sincerely acknowledge the mentorship and support that my supervisor, Assist. Prof. Dr. Ghulam Hussain has extended throughout my MS program. It wouldn't have been possible to succeed without his enthusiasm for research, and the excellent guidance.

I want to show my appreciation to my co-supervisor, Assist. Prof. Dr. Mostafa Ranjbar**,** for the support and guidance has extended throughout my research progress.

I wish to thank all the faculty members and staff of Mechanical Engineering Department for their continued cooperation. I would like to thank all my friends, for their support and encouragement especially graduate students Khosro Bijanrostami and Reza Hashemi.

I would like to thank my wife, my parents and other family members for providing the motivation and support for pursuing my master's degree. It would have been impossible without the support and encouragement of my parents to achieve this degree.

`

TABLE OF CONTENTS

`

`

LIST OF TABLES

`

LIST OF FIGURES

`

`

LIST OF SYMBOLS/ ABBREVIATION

AA	Aluminum Alloy
Al	Aluminum
ANN	Artificial Neural Network
ASTME	American Society for Testing and Materials
C	Carbon
CNC	Computer Numerical Control
Cr	Chromium
Cu	Copper
°C	Degree Celsius
DVOM	Digital Volt-Ohm meter
F	Feed Rate [mm/min]
Fe	Iron
FS	Friction Stir
FSP	Friction Stir Process
FSW	Friction Stir Welding
GA	Genetic Algorithm
GMAW	Gas Metal Arc Welding
GTAW	Gas Tungsten Arc Welding
g/cm^3	Gram per Cubic Centimeter
HAZ	Heat Affected Zone
HRC	Hardness Rockwell Scale
HV	Vickers micro-hardness
I	Electric Current [Amp]

`

kWh	kilowatt hour
Mg	Magnesium
mm	Millimeters
Mn	Manganese
MPa	Mega pascal
N	Tool rotational speed [rpm]
Ni	Nickel
Si	Silicon
T	Time [s]
Ti	Titanium
TMAZ	Thermo-mechanically affected zone
TWI	The Welding Institute
UTS	Ultimate Tensile Strength
V	Voltage [v]
YS	Yield Strength
Zn	Zinc
Φ	Machine power factor

`

Chapter 1

INTRODUCTION

1.1 Characteristics and Applications of Aluminum 7075-T651 Alloy

Aluminum is a soft, low cost and very lightweight metal with a specific weight of 2.70 g/cm^3; about one third that of copper played an important role in modern industries. It presents well from very low temperatures to moderate temperatures and it has a high strength-to-weight ratio. Aluminum naturally makes a protective oxide coating and highly corrosion resistant. At subzero temperatures their strength increases besides their strength decreases if they are subjected to high temperatures, this property is particularly useful for applications where protection and conservation are required. In addition to the advantages cited above other properties of aluminum include: high electrical and thermal conductivity, ease of fabrication, high reflectivity and 100% recyclable with no downgrading of its previous qualities. These beneficial properties have made more industries to gradually change steel products to aluminum products. Figure 1.1 illustrates the importance of aluminum in our new era[1].

The wrought Aluminum alloys (AA) are heat treatable alloys; the strength of these alloys can be increased to very high levels by age (precipitation) hardening. In table 1.1 designations for aluminum wrought alloys are mentioned. The 2XXX and 7XXX alloy series are the major groups of alloys in aircraft industries for airframe parts especially where the high strength is the primary design parameters such as fuselage skin and upper wing skins. The 7XXX alloys are very responsive to age hardening

`

and are artificially aged to the peak strength T6 (Solution Treated + Artificially Aged) or the overaged T7 conditions.

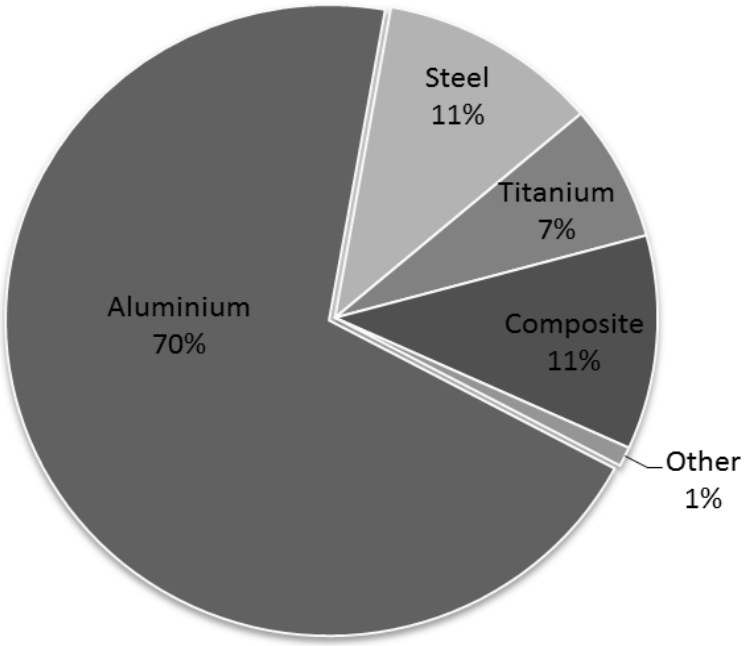

Figure 1.1: Material Distribution for Boeing 777 Aircraft [1].

Welding 7XXX alloys with usual welding processes can be difficult; however some of them are weldable by conventional methods such as Gas Metal Arc Welding (GMAW), Gas Tungsten Arc Welding (GTAW), and resistance welding. A new welding process, Friction Stir Welding (FSW), offers the ability to weld the difficult 7XXX alloys. The major traits of the 7XXX series are heat treatable, typical ultimate tensile strength range (220-600 MPa), very high strength, and mechanically joined. In this study AA7075-T651 is used. One of the highest strength aluminum alloys available; that the major impurity elements in this alloy are zinc with some copper, magnesium, and low quantities of chromium and manganese. Its strength-to-weight ratio is excellent, and used for highly stressed parts where strength is design driver. Due to their high corrosion resistance and high strength, these alloys are extensively

`

used in air craft fitting, missile parts, aerospace and defense equipment and components as a structural material.

Table 1.1: Designations for aluminum wrought alloys [1].

Series	Al content or main alloying element
1XXX	99.00% Minimum
2XXX	Copper
3XXX	Manganese
4XXX	Silicon
5XXX	Magnesium
6XXX	Magnesium and Silicon
7XXX	Zinc

1.2 History of Friction Stir Processing

Finding fitted material based on the application is the primary and the most important parameter in industrial design. This parameter is more prominent in the automotive and aircraft industries. However, processing of such materials with desired properties has certain limitations in terms of cost and time of production, aside the reduction in ductility. Prerequisite of having material with properties like high ductility and high strength is to possess fine and homogenous grain structure in their alloys. In order to find a processing technique that satisfies these requirements as well as the cost and time of production, the new processing technique named Friction Stir Processing (FSP) has been developed. FSP is a new thermomechanical and solid state processing technique that a development based on FSW initially developed by The Welding Institute (TWI) in United Kingdom [2,3]. FSW is a development in metal joining and has been successfully used to produce joints in aluminum, titanium and other alloys.

`

It is evident that FSP and FSW share the same mechanism but their applications have different purposes. The aim of FSW is to join two plates together, whereas FSP aims at modifying the microstructure of a workpiece.

Some of the advantages of FSW are mentioned in the following list [4]:

- This process is energy efficient.
- Comparing with other processes it requires minimal consumables.
- Aside of welding and joining plates FSW produces desirable microstructures in processed zones.
- During FSW no fumes, noise or sparks occur so it is totally the environmentally friendly welding process.
- With the help of FSW, joining materials that are unweldable by conventional welding methods will be possible.

1.3 Principle of FSP

In the near past, a new property modification method called as FSP was invented. This employs a specially designed cylindrical rotating tool consisting of a pin and concentric larger diameter shoulder to process the material. The pin after plunging, stirs the material and the shoulder performs consolidation by applying pressure. Depth of penetration was controlled by the tool shoulder and length of the pin. The rotating pin contacts the workpiece surface and friction between the sheet surface and the tool shoulder rapidly generates frictional heat. This results in severe plastic deformation and recrystallization of the material which is forced to flow from the forward end to the trailing end as the tool advances. The recrystallization is restricted to the localized zone and is performed in a dynamic manner. Schematic drawing of friction stir processing is given in figure 2.1.

`

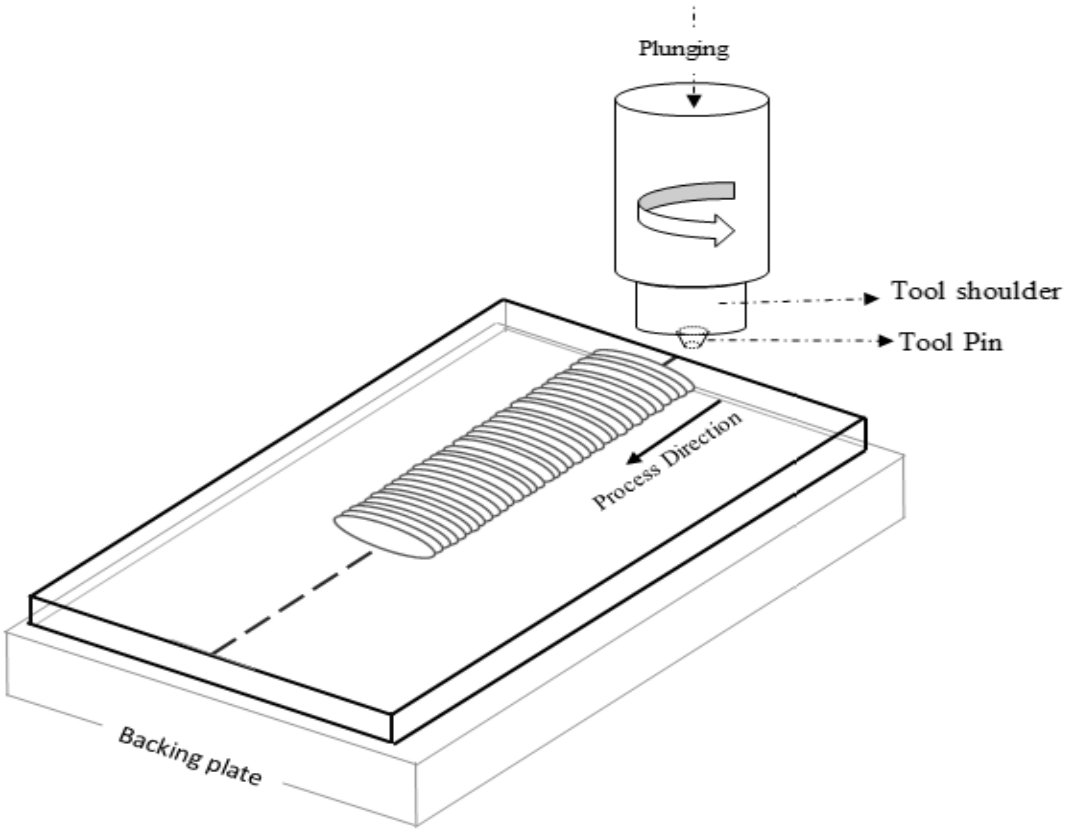

Figure 1.2: Schematic drawing of FSP.

The temperature during FSP has been observed to be below the melting point of the material, thus the material during processing remains in solid state. Although FSP was advanced as a grain refinement technique, it has found several other applications including rectification of defects in castings, mechanical alloying and surface modification to improve wear and lubrication characteristics [5,6].

1.4 Artificial Neural Networks

In this thesis, optimization of FS Processing of aluminum alloy by using genetically optimized neural network is presented. Artificial Neural Networks (ANN) algorithm is proposed to make an approximation from the real objective functions.

ANN is an information processing model and a complicated system composed of numerous nerve cells, such as brain, that is inspired by biological nervous systems [7]. They have been developed to train virtual networks of computer system which is

`

based on the primary understanding of the organization, structure, function and mechanism of the human brain for the approximation of the computational expensive real world objective function based on some initial design data. So whenever it is necessary by using this trained network we can calculate the value of objective functions. Calculations by ANN are very cheap and so they can be considered as a suitable alternative for the replacement of function approximation.

1.5 Definition of the Problem

To obtain high efficiency of a material processing technique, there is a need to maximize the properties and minimize the cost. These objectives are often in mutual opposition. Analytical methods cannot solve such issues. This is the situation where experiments based methods such as empirical modelling and computational intelligence come into play. In the present study, the suitability of ANN and Genetic Algorithm (GA) to optimize FSP will be examined.

1.6 Objective of this Study

The aim of this work is to explore this open research area and relatively trade-off among mechanical properties and energy consumption in multi-pass FSP of AA7075-T651 aluminum employing hybrid approach of ANN and GA. At this regard, the global approximation scheme ANN is used in combination with the GA method to perform a multi-objective multivariable optimization process. The specific objectives of the study presented are:

i. Quantify the effect of variation in FSP parameters on mechanical properties of AA7075-T651 alloy.
ii. Study the role of FSP parameters on energy consumption during the process.
iii. Develop an ANN based on our experimental data.

`

iv. Establish the global approximation scheme ANN in combination with the GA method to perform a multi-objective multivariable optimization process.

1.7 Thesis Organization

This study is presented into five chapters. First chapter includes an introduction of the workpiece material AA 7075-T651, FSP, ANN and their applications. Chapter 2 has overview of earlier studies and works done related to our work. Experimental methodology used for obtaining the results mentioned in the third chapter. Fourth chapter includes the results that obtained during the experiment. Finally Chapter 5 will give conclusion of our study and suggest some future works that can be done further in order to make this study complete.

`

Chapter 2

LITERATURE REVIEW

This chapter reviews the earlier works and researches that have been done related to our study.

2.1 Friction Stir Processing Technology

FSP is a modification of friction stir welding innovated by Mishra et al. [5,6]. This processing technique is used to modify microstructure of metals concerning change grain size, uniform structure of grain size, and increasing strength and surface composites. Mishra et al. [6,8] reported the optimum superplastic strain rate to be 10^{-2} s^{-1} at 490 °C achieved in FS processed AA 7075 sheet. Besides, Mahoney et al. [9] presented friction stir processing as a thermo-mechanical process to create a fine grain microstructure in thick section (>5mm) of Al 7050-T651 which resulted in high strain rate super-plasticity. Mishra et al. [10,11] also in another study, by expanding this process, reported that other applications such as producing surface composites, modifying the microstructure of selective location produced by powder metallurgy, and refining microstructure in metal matrix composites, improve properties of casting alloys. Hsu et al. [12] indicated that production of Al/Al_3Ti nanocomposite can increase the young's modules and tensile strength of aluminum and also they found out that young's modules will develop through increasing the percentage of Al_3Ti.

`

FS processed zone can be divided into four distinct regions, defined and demonstrated (Figure 2.1) as follows [1]:

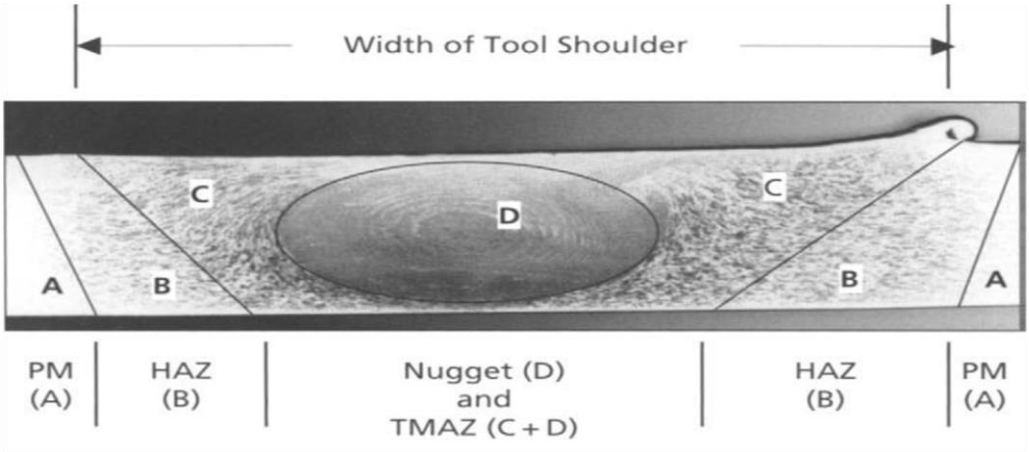

Figure 2.1: Schematically drawing of FSP zones [1].

Where, (A) is Parent metal (Unaffected material), this part of material is located far away from process so that it has not been deformed during FSP and is not affected in terms of mechanical and microstructure properties, (B) is Heat-affected zone (HAZ), this part is closer to the center of the FSP and no plastic deformation occurs in this region although it has experienced a thermal cycle that has modified mechanical properties as well as the microstructure.

Distinct (C) is Thermomechanically affected zone (TMAZ), this part is located under the FSP tool and has deformed the material plastically. Moreover, the frictional heat generated during the process has exerted some effect on the material structure and part (D) is Stir Zone (Recrystallized Nugget), this part is related to the trace of the tool pin that traverses through the material and is a fully recrystallized and homogenized area.

`

2.2 Process Parameters and Properties during FSP

The major process parameters that affect the performance of FSP are: transverse (f) and rotational speed of spindle (N), pass quantity and tool geometry. This section gives an overview on how process parameters influence the properties of the processed material in the field of FSP to be considered for controlling the process. These parameters are process controllers which have a major effect on the microstructure of the processed zone [13].

2.2.1 Rotational Speed of Spindle and Feed

Frictional heat and mixing (stirring) the material around the pin will be generated by the rotation of the tool on the surface of the material. Pin feed also transfers the material from the advance part of the pin to its back part. By increasing this factor (N), mixed material will increase while also heat is generated, however, there will be a change in the friction coefficient of the surface while factor (N) increases [14].

Through heat grain growth rise throughout recrystallization, grain size also grows. But there would be a reduction in the grain size as a result of feed rate growth. The reason is that when feed rate increases, material's process period and its produced heat decreases which leads to grain growth decline while recrystallization as well as a decrease in the grain size [15].

For achieving a fine structure, there should be a reduction in the rotational speed while increasing the feed rate, however, when applying this parameters, it should be noted that heat is also generated less as a matter of which heating may be needed to soften the material, besides, plastic deformation also can be obtained in a smaller amount [14,15].

`

Gharacheh et al. [16] also have reported that different traverse or rotational speed ratios can have different effects on mechanical properties in different zones. According to their study, increasing the ratio mentioned above causes a small decline in the stir and transitional zone's yield and their ultimate strength. Moreover, they had detected that when traverse or rotational speed ratio increases, the size of weld nugget upsurges as well while the incomplete root penetration declines. The reason behind these issues is that in these regions, heat input rises and the material softens. Moreover, when there is a rise in heat input and when the material flow is easier, a larger weld nugget is shaped because of the increase in N/f ratio. As a result, when N/f ratio rises, there will be a reduction in the probability of shaping an "incomplete root penetration" defect.

El-Rayes and El-Danaf [17] studied the influence of first three parameters on the properties of Al-6082T651. They found that there is an increase in the mean grain size when passes (with 100% overlap) from 1 to 3 and the feed from 90mm/min to 240mm/min increase. However, the hardness and strength reduced as the passes increased while both of these quantities increased as the feed increased.

Further, the effect of tool rotation (850rpm to 1350rpm) was observed to be insignificant on the mechanical properties but the mean grain size was noticed to increase. Karthikeyan et al. [18] investigated the impact of rotational speed (1400rpm to 1800rpm) and feed (10mm/min to 15mm/min) on the mechanical properties of casted Al2285 to show that the increase in the feed caused a gradual decrease in the strength and elongation and contrarily increase in the micro-hardness. An increase in the rotational speed, on the contrary, improved all of the properties. Moreover, for any set of parameters, each of the tested property of FS Processed material was

`

perceived to be greater than the corresponding property of the base metal. For AA319 casted aluminum, Karthikeyan et al. in another study [19] found that there was certain combination of parameters (i.e. 40mm feed and 1200rpm speed) which yielded the best properties by de-voiding the casting.

2.2.2 Overlapping

Ma et al. [20] applied single pass FSP on the cast A356 alloy, figuring out that the FSP has caused significant break up of Si particles and dendrites. Further, variation in the considered FSP parameters (i.e., feed from 51mm/min to 203mm/min and rotational speed from 300rpm to 900 rpm) did not substantially affect the size of grains. They [21] further studied the effect of 5 passes (with 50% overlap) and observed that overlapping FSP did not have a significant impact on Si particle distribution. Further, the strength and ductility of single pass alloy was comparable to those of 5-passes alloy. Johannes and Mishra [22] with an aim to improve the superplastic behavior performed 4-pass FSP (with 42% overlap) on Al7075 alloy and found that the pass-grain size relation was non-linear. The finest grain size was obtained with 2-passes and the highest elongation was shown by 1-pass sample at 743K temperature.

Bauri et al. [23] applied single and double pass FSP for the fabrication of Al/TiC composite. In agreement with [24], it was found that the double pass FSP yielded composite with improved properties. Faraji and Asadi [25] reported that a large ratio of speed and feed along with higher passes reduced grain size and increased hardness and wear resistance of the AZ91/alumina composite. Zohoori et al. [26] for Al5083/Cu composite found that both the strength and hardness increased when there was a raise in rotational speed from 700 rpm to 1900 rpm.

`

2.2.3 Pin Geometry

Of the elements which play a critical role in friction stir technology is tool design. As a result, to make the process more effective, this area of study should be emphasized more. Only a few contributions have been given in this study area, which are as follows. The key to applying the process effectively to a wider range of materials and also over a greater range of thickness is the tool design. Hence, there have been studies on some different enhanced tool designs. For example in a study conducted by Thomas et al. [27], recent developments were described which have used these high performance tools from the point of view of present and potential applications.

Azizieh et al. [24] studied the effect of pin geometry, number of passes and rotational speed on the hardness and grain size of the AZ31/Al_2O_3 composite. Of three columnar pin geometries (i.e., without threads, with threads and with threads and 3 flutes), it was found that only the composite fabricated with the threaded pin was free from defects because of better material flow. When the passes increases, grain size is reduced while the hardness increases. On the contrary, when the rotational speed increases, the hardness decreases despite the fact that there is an increase in the grain size. The highest hardness was achieved with 800 rpm and 4-passes with the threaded columnar pin. They reported that increasing the passes quantity enhanced the hardness by improving the distribution of Al_2O_3 particles in the AZ31 matrix. A similar result was observed for the Al5052/Al_2O_3 composite [28]. The ductility however was found to decrease after the 3rd pass. The authors emphasized to employ large rotation to feed ratios to produce defect free composite. While comparing the performance of 5 different pin geometries including square, triangular, four-flute cylinder, four-flute square and threaded taper, Bahrami et al. [29], contrary to threaded pin in [22], found that the triangular pin showed the best performance in

`

terms of grain refinement, particle agglomeration (a defect) and properties during fabrication of SiC/Al7075 composite.

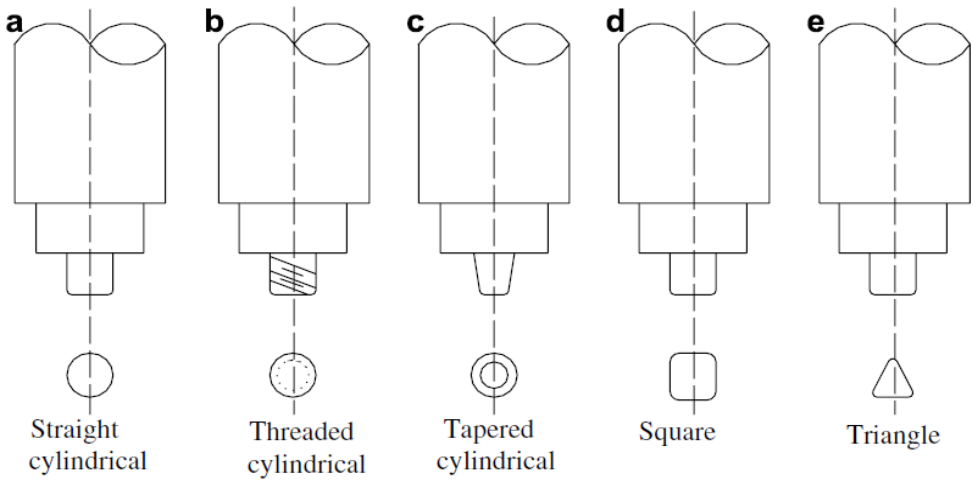

Figure 2.2: Different types of pins [30].

2.3 Artificial Neural Network

A computational model has been developed by McCulloch et al. [31] for the neural networks grounded on algorithms and mathematics. Thereafter, a learning model was created by Hebb [32], based on neural plasticity mechanism.

Also an algorithm was created by Rosenblatt [33] on the grounds of a two-layer learning computer network for recognizing the patterns. However, until after Werbos [34] generated the back propagation algorithm, Rosenblatt's algorithm could not be processed, using an easy addition and subtraction approach. As basic models of neural processing in the human brain, artificial neural networks can be taken into account. Nevertheless, there are discussions on the relationship between brain biological architecture and this model, for the degree to which these artificial neural networks can reflect brain function is not clear [35]. Thereafter, for biophysical simulation devices, computational platforms were produced [36, 37]. For design

`

problems, these platforms can make the neural network modelling procedure easier for problems in great scales.

2.4 Multi Layers Neural Network Function Approximation

A sort of Artificial Intelligence method, imitating human brain behavior is artificial neural network (ANN) [7]. This technique, unlike most traditional statistical methods, has the capability of modeling non-linear and linear systems deprived of the requirement for indirectly making assumptions. In the links between specific nodes of the network, weight factors are adapted in order to have complemented expected and generated output data. When training is completed, the network can substitute an original one, being used like an easy function. Arslan et al. [38] proposed a procedure for subsequent usage of artificial neural networks (ANN) in general. A neurobiological method is imitated by neural network, treating the input and producing the output. This technique can be accomplished by a couple of input and output figures.

When there is no way for analytically explaining the problem, application of ANN method is more appropriate. The effectiveness of the redesign process can be enhanced by a trained network where quick plotting of the input given into the favorable output quantities is available. The following tasks are included in ANN training. Firstly, an appropriate training set should be selected, then proper network architecture should be established and afterwards, suitable values of characteristic constraints such as momentum term and learning rate should be determined [39]. Ranjbar and Marburg [40] showed the application of a hybrid method including of artificial neural network and simulated annealing methods.

`

2.5 Multiobjective Optimization by Genetic Algorithm

Evolutionary algorithms encompass different approaches which are also named as evolutionary computation approaches, including: evolutionary programming, genetic programming, genetic algorithms, differential evolution, and evolution strategies. Genetic Algorithm or the GA is a model based on both the Darwinian "survival of the fittest" theory and gene recombination [41]. That means if the ability of a group of individuals to succeed in the environment (fitness) is high, they have a better chance for reproducing in that environment. Broods are created through a crossover process (combining genes) and transformation [42]. Also, Kalyanmoy published a book on Multi-Objective Optimization via Evolutionary Algorithms [43].

Principal operations in a GA are as follows [44]:

i. Broods are created via the crossover process from two individuals selected from the population, through some bits being exchanged between the two. That is why some characteristics are inherited to the broods from each parent;
ii. One or several bits in an individual are changed randomly in the transformation operation to create an infant. Hence, broods own diverse characteristics from their parents. For solving the premature convergence problem, the transformation machinist is considered an essential element, because this mechanist assists in making random diversity in the population;
iii. According to predefined procedures, broods are chosen for survival by the selection process. In this way, population size is kept within a fixed constant and there is a higher probability that the next generation owns better broods.

`

The above short review reveals that the process parameters in FSP significantly affect the process performance in terms of properties and defects. Furthermore, the nature of influence of a particular parameter is substantially dependent on the type of material under investigation. Besides the properties and defects, another important performance measure which yet has not been addressed in FSP is energy consumption, minimization of which is important not only to control cost but also for the environmental protection. The effect of a parameter, as reported above, on performance measures could be in mutual opposition. Therefore, to maximize the FSP efficiency, the parameters must be opted judiciously, and such a task normally requires trade-off among various performance measures of the process. In literature, such works have been reported for other manufacturing processes like machining, friction stir welding and metal forming [45-50]. However, to the best knowledge of the authors, any similar study on FSP, especially related to Al7075, is not available.

To achieve an improved product competency in terms of both cost and performance, the design requires the use of a material with high values of strength, hardness and ductility. Intrinsically, a material having high strength possesses low ductility. For reducing the product cost, the energy consumed in manufacturing a material is also a matter of concern. This study, employing FSP as a material processing tool, attempts to explore the most suitable parameters satisfying these objectives for Al7075. Seemingly, the requirements of the stated goals, in terms of settings of the process parameters involved, are expected to be in mutual opposition. Moreover, almost all the manufacturing processes involve complex physical, chemical and metallurgical phenomena, which render them impossible to be modeled analytically within acceptable levels of accuracy. This is the situation where the experiments based methodologies, for example statistical empirical modeling and computational

`

intelligence, come into play. Empirical models have their own limitations because as the number of parameters increase and experimental database grows, the models become more complex, inaccurate, and inapplicable [51]. Therefore, the most feasible option available in such a situation is computational intelligence (e.g. artificial neural networks).

`

Chapter 3

METHODOLOGY

In this study we intend to experimentally investigate the effects of various process parameters on the Mechanical properties and energy consumed during FSP of aluminum 7075-T651 plate.

In this chapter an overview of the material, experimental setup and procedure of our study would be given.

3.1 Workpiece Properties

A wrought AA 7075-T651 plate with 5mm thickness is used as the experimental material as designated in first chapter; properties of this material outlined in the following tables. Table 3.1 stands for the chemical structure and table 3.2 physical and mechanical characteristics of the AA 7075-T6 tabulated.

Table 3.1: Chemical structure of the AA 7075-T6 [52].

Element	Al	Cu	Mn	Mg	Cr	Ni	Zn	Fe	Si	etc.
Content (%)	Base	1.55	0.15	1.4	0.2	0.01	4.9	0.18	0.06	0.26

AA 7075-T651 sheet with dimensions of 1000*2000*5 mm was cut into 140*50*5 mm sample size plate using guillotine showed in Figure 3.1 cutting process was done in the way in the rolling course of the first sheet is the length of sample sheets and in the course of sample length, FSP was done.

`

Table 3.2: Properties of AA 7075-T6 [52].

Property	Value
Thermal conductivity	130 W/m-k
Electrical resistivity	5.15e-006 ohm-cm
Density	2.81 g/cc
Melting point	477-635 °C
Crystal structure	FCC
Machinability %	70%
Elongation at break %	11%
Modulus of Elasticity	71.7 Gpa
Shear modulus	29.6 Gpa

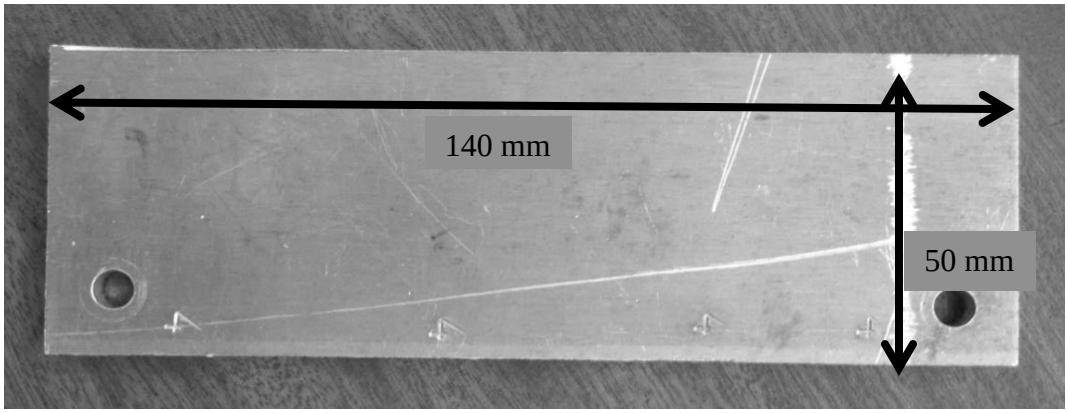

Figure 3.1: Initial shape of workpiece.

3.2 Experimental Setup

The experimental setup required to FSP aluminum alloys is discussed in this section. The schematic of multi-pass FSP for the current investigations is shown in Figure 3.2.

`

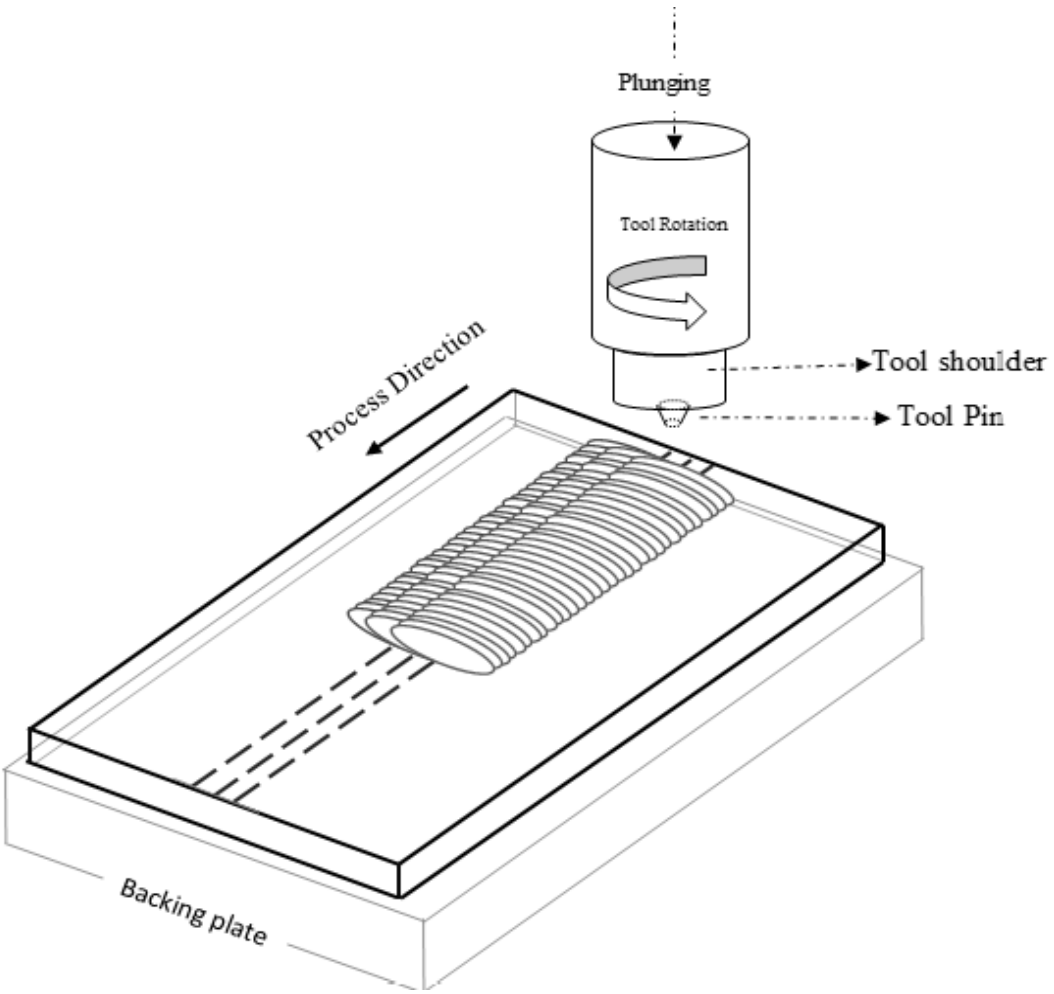

Figure 3.2: Schematic view of multi-pass FSP.

3.2.1 Friction Stir Processing Tool

A steel tool with 50HRC hardness and threaded taper pin with 1mm pitch size, 0.5 mm thread depth, 15 mm shoulder diameter and 2.5 mm pin height was employed as the stirring tool, Figures 3.3(a) and (b), shows the FSP tool.

3.2.2 Equipment of the FSP

On a conventional vertical milling machine, the process was accomplished with counter clock wise rotating direction showed in Figure 3.3(c), which by clamping a vice on machines table that can fix work-piece and prevent sliding and movement of sheet under process force while backing plate made of steel is placed on the fixture to support the FS processed sheet during the process.

`

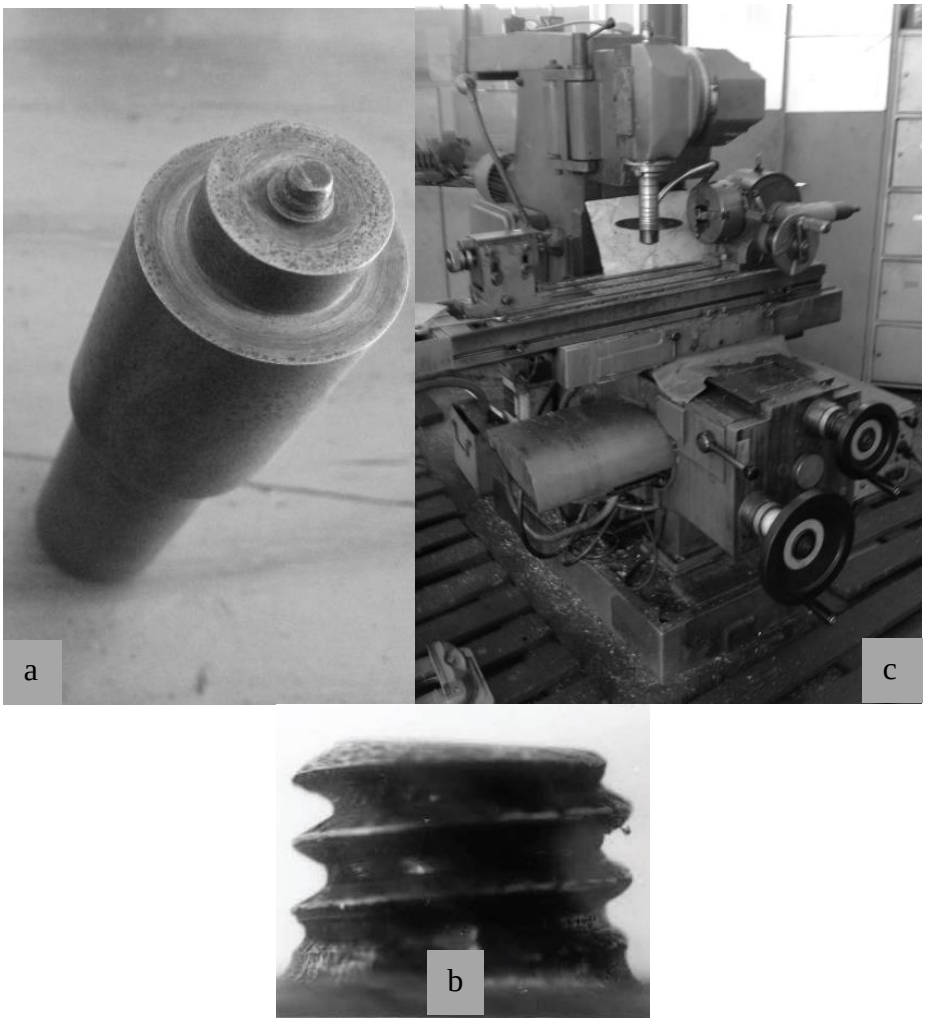

Figure 3.3: (a) Processing tool; (b) Threaded taper cylindrical pin; (c) Picture of milling machine used for friction stir processing.

3.2.3 Machine Settings

The angle between workpiece normal and spindle (tool spindle angle) of 2.5 degree was fixed and used for all samples that at the straggling edge of the shoulder, it assists in forging the action.

The target depth (depth of penetration) has been clarified as being the amount of deepness the pin will go into the work-piece. Concerning the top surface of the work-piece, target depth can be controlled by the shoulder. In this work 0.2 mm depth of

`

penetration was held fixed. Figure 3.4 illustrates schematic view of these two fixed parameters.

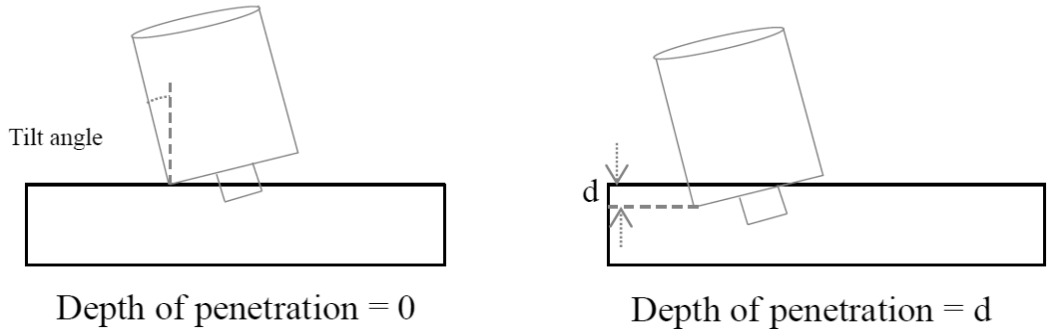

Figure 3.4: Figure of Tool penetration.

3.3 Experimental Procedure

According to the machine limit 8 samples were FS processed by various values of feed (f) and rotational speed (N) in a way that cover important points of our network. Demonstrated in Table 3.3, each parameter was varied over four levels. The samples were produced employing three passes with 50% overlap, in the other word there is 3mm spacing between pin centers of the tool for each pass.

Table 3.3: Test data sets of Sample

Samples	1	2	3	4	5	6	7	8
N (Rpm)	500	500	500	710	1000	1000	1400	1400
f (mm/min)	63	160	250	250	63	160	63	100

`

Table 3.4: Test plan and comparison of parameters range opted in the present and previous studies.

Spindle speed (rpm)	Feed (mm/min)	Fixed parameters	Range of parameters: comparison		
			Parameter	Current study	Previous studies
500	63	Pin diameter: 5mm	Feed (7075)	63-250	[17] 90-240 (6082-T651)
500	160	Pin height: 2.5mm			[18] 10-15 (2285- casted)
500	250	Shoulder diameter: 15mm			[21] 51-203 (319- casted)
710	250	Tilt angle: 2.5^{o}			
1000	63	Penetration: 0.2mm	Speed (7075)	500-1400	[17] 850-1350 (6082-T651)
1000	160	Tool hardness: 52-55HRC			[18] 1400-1800 (2285- casted)
1400	63	Tool material: H13 steel			[21] 300-900 (319- casted)
1400	100				[24] 800-1200 ($AZ31/Al_2O_3$)

3.4 Energy Consumption during FSP

Among the key components of a FSP machine are feed-axis motors and spindle. Used up electrical energy transforms to supplied mechanical power by a machine's network of drives. Drive network apparatuses are drive modules, a power supply module, mechanical components, and motors.

With the help of Digital Volt-Ohm meter (DVOM) devices, current (I) and voltage (V) was measured during the process. Time consumed (sec) in completing a sample is dependent on sample set traverse speed and measured by a stopwatch, after collecting data for each set energy consumption was computed using the following relation:

`

$$kWh = (\sqrt{3} \times V \times I \times \cos(\phi) \times \frac{t}{3600} \times 10^{-3} \qquad \text{[57] Equation (3.1)}$$

Where kWh is energy measured in kilo watt hour, V is voltage [V], I is current [Ampere], t is time consumed [s] and Φ is power factor which was 0.7 for the machine tool employed in this work. The cost of one kWh electrical energy consumed is assumed to be 0.50 Turkish Lira (0.25 $) as the reference.

3.5 Hardness

The most common testing technique for evaluating localized mechanical characteristics is hardness testing. Hardness test specimens were cut in direction that is perpendicular to the traverse process direction, then specimen's surface clearly sanding to remove the swarfs and obtaining smooth surface. The micro-hardness of each sample in the nugget zone was determined using the Vicker hardness tester by WOLPERT WILSON INSTRUMENTS machine (Fig. 3.6 (a)). In this test, the practical load was 98.1 N (HV_{10}), with 10 seconds dwell time and 15 seconds test time. The diameter of automatically results and the effected point measured, using the measuring and optical equipment on the machine, were demonstrated on the device monitor. Figure 3.5 shows the picture of hardness test specimen and Figure 3.6 shows the micro-hardness tester.

Figure 3.5: Hardness test specimen.

`

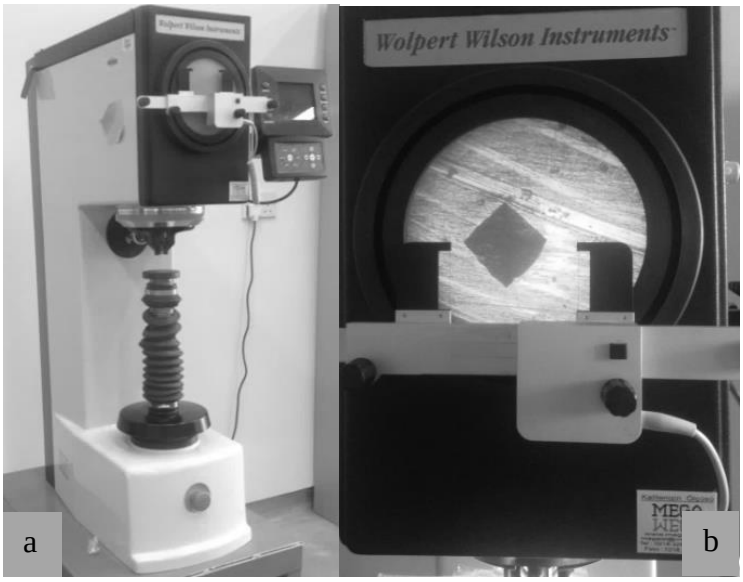

Figure 3.6: (a) Micro-hardness tester. (b) Optical and the measuring equipment.

3.6 Tensile Test

The mechanical properties of the processed material were determined through a tension test, evidence regarding the elongation and ultimate tensile strength (UTS) of the processed samples. The sub-size tensile specimens according to the ASTME8 standard [53] (Fig.3.7) were cut along the processing direction by a DUGARD EAGLE 760 CNC machine as shown in Fig. 3.8 (b) and stretched to fracture using INSTRON tension machine (Fig. 3.8 (a)). For the tensile tests, the nominal strain rate was $1\times10^{-3}\,s^{-1}$.

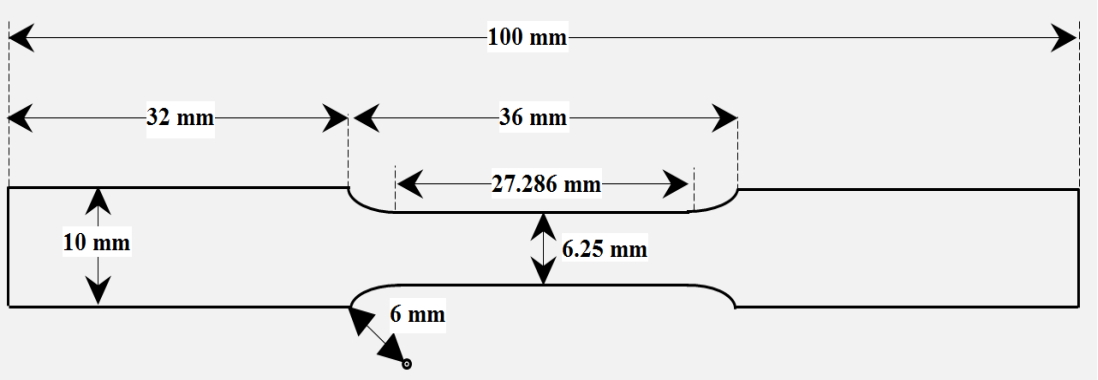

Figure 3.7: Sub-size ASTM E8 standard tensile specimens.

`

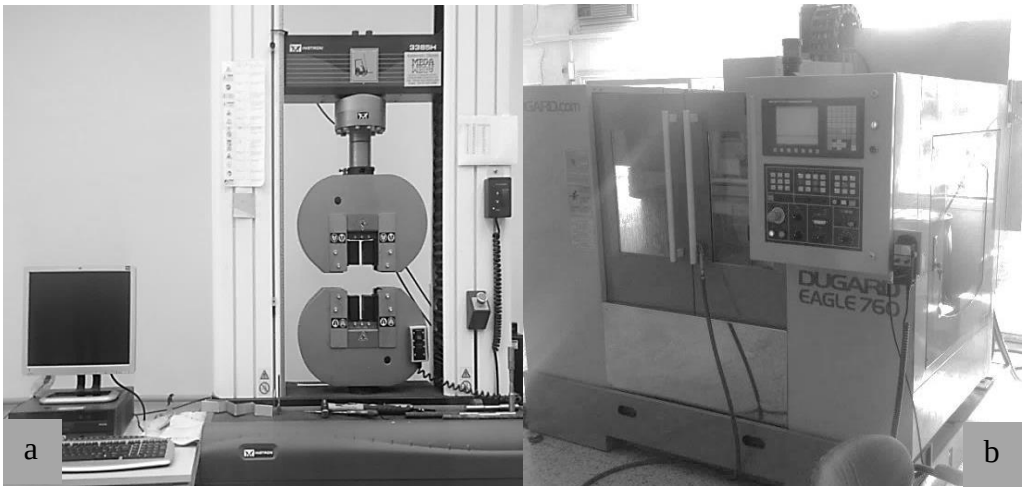

Figure 3.8: (a) The tensile test machine (b) CNC cutting machine.

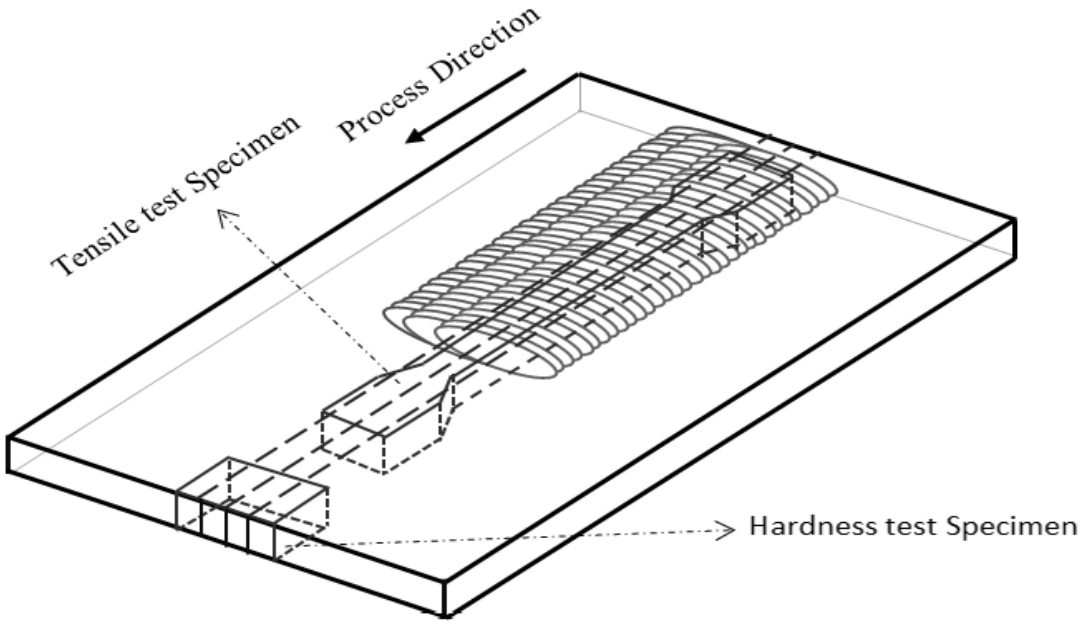

Figure 3.9: Cutting plan for tensile and. micro hardness test's specimens.

3.7 Optimization procedure

In this section, the approximation of function by ANN and the procedure for multi-objective optimization of FSP will be presented.

3.7.1 Multi layers NN function approximation

In the links between specific nodes of the network, weight factors are adapted during this training time so that the expected and generated output data match. The network,

`

after being trained, can substitute the original one, being used as a simple function that s. There is actually no analytical relationship between the inputs and outputs of FSP. Therefore, only a numerical solution is possible. To compute a numerical model from the objective tasks, ANN is used. ANN trains couple of neurons to substitute the chief objective functions. Hence, some training affiliates such as the chief objective function's values in quite a few distinct design points are experimentally measured. Thereafter, to simulate the chief objective function practically, neural network gets trained. As a result, in a shorter period, trained objective function can be premeditated compared to the other methods, plus limited elements analysis. Fig.3.10 depicts the general structure of ANN with several inputs, hidden layers and neurons. The trained multi-layered perception network will approximate the value of outputs with respect to given inputs.

Four ANN are considered for the representation of friction stir processing. Feed forward scheme is used for ANN modelling. The value of elongation, tensile strength, hardness and cost of consumed energy are approximated by ANNs. The inputs of ANNs are the rotational speed of spindle and feed rate of tool, see Fig. 3.11. Four neural networks are used to approximate the values of elongation, ultimate strength, hardness and cost of energy consumption. These neural networks are trained based on the experimental data.

`

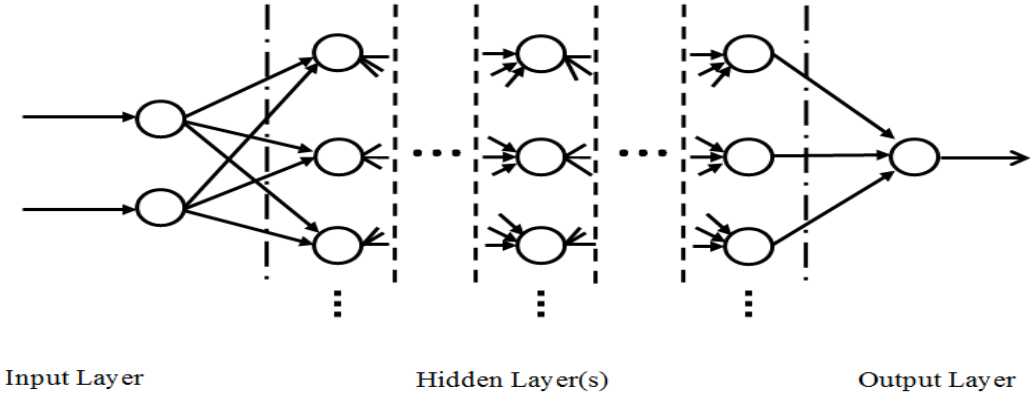

Figure 3.10: A multi-layered perception network

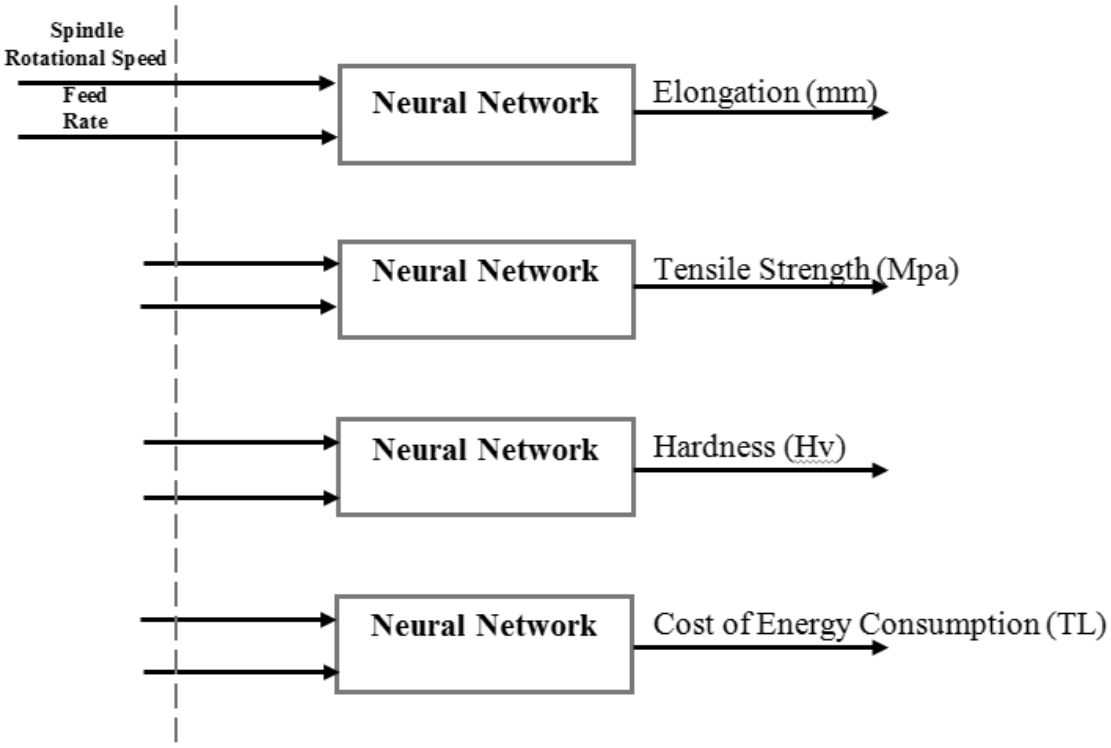

Figure 3.11: Four Artificial Neural Networks for representation of the FSP.

3.7.2 Neural Network-Based Multi-Objective Genetic Optimization of FSP

When an ideal solution is gained, a single objective optimization algorithm will typically be ended. Yet, there can be numerous ideal solutions for supreme realistic multi-objective problems. Depending on some factors such as problem environment and user's choice, suitability of one solution can change, which is why it is preferred to find the whole set of ideal solutions.

`

A common multi-objective optimization problem mathematically includes underrating several objectives as well as satisfying (optional) constraints. Respectively, a multi-objective optimization problem involves the following criteria:

Maximize: Hardness, Elongation, and Ultimate Tensile Strength.
Minimize: Cost of consumed electrical energy for FSP, with respect to the rotational speed of spindle and feed rate of process.

Having a vector of decision variables which can optimize all the objectives at once is challenging for what is meant by optimum is not clear in this context. Hence, Pareto optimality concept is used. However, this concept cannot be directly pertinent from single objective to multi-objective optimization problems. As a result, based on the following definitions, solutions are classified regarding Pareto optimality [54].

In fact, a family of similar solutions is available which are greater than the other solutions in a common multi-objective optimization problem, that from the simultaneous optimization viewpoint of multiple and probably opposing objective functions, they are considered identical. These kinds of solutions are named Pareto-optimal solutions. It should be noted that without corrupting at least one of the other Pareto-optimal solutions, no objective can be developed, and also there is no solution available elsewhere than the true Pareto front, considering the model constraints.
Locating the entire Pareto front is the goal of multi-objective algorithms. Concerning a bi-objective space, in Figure 3.12, a representation of the Pareto front is shown.

`

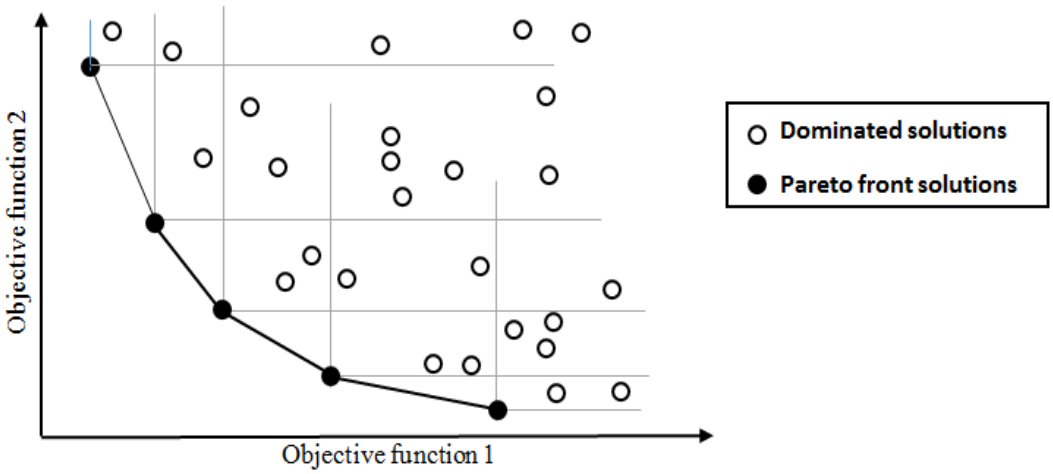

Figure 3.12: The Pareto front of a set of solutions in a bi-objective space [55].

In this study, the number of genetic population is considered to be 50. Also, the values of 0.8 and 0.35 are considered for the cross over fraction and Pareto fraction. The maximum number of generations in genetic optimization is set to be 400.

The schematic flow chart of multi-objective neural network-based optimization process is shown in the Figure 3.13. In each generation of genetic optimization, the approximated values of elongation, tensile strength, hardness and cost of energy consumption by ANN are using to form the population. The multi-objective genetic optimization continues until when there is no distinct change in the Pareto front of set of solutions. Then, the optimum value of spindle rotational speed and feed rate will be reported.

`

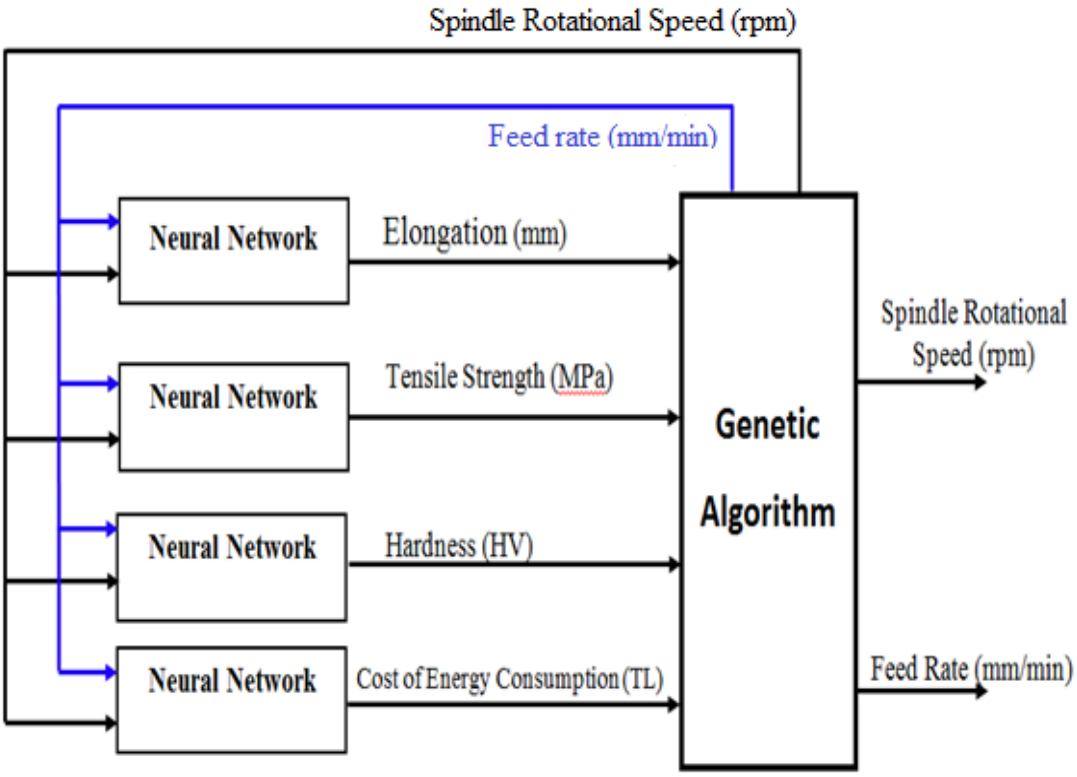

Figure 3.13: General flow chart of artificial neural network-based multiobjective multivariable optimization of FSP.

The internal controling parameter values for neural networks approximation method and genetic algorithm have been selected from Ranjbar et al. [35] and Ranjbar [56]. In next chapter, the results of multiobjective multivariale neural network-based genetic ootimization of FSP will be presented.

`

Chapter 4

RESULT AND DISCUSSION

In the present study, the effect of two major process parameters (namely rotational speed and feed) on three mechanical properties and energy cost employing Al7075-T651 has been studied. The ANN as a virtual function approximation tool and GA method as an optimization tool to simultaneously achieve the objectives of improving mechanical properties and lowering the energy cost will be employed.

4.1 Producing Samples

The figure 4.1 shows one of the processed samples while the spindle is located at the end of the first pass and figure 4.2 (a) and (b) shows the number 2 and 5 set samples processed surface respectively.

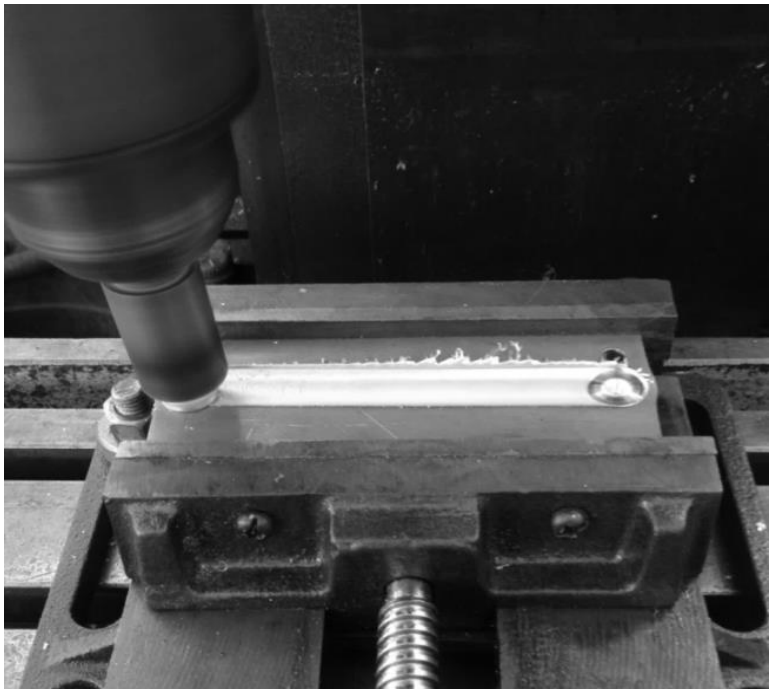

Figure 4.1: FS Processed sample

`

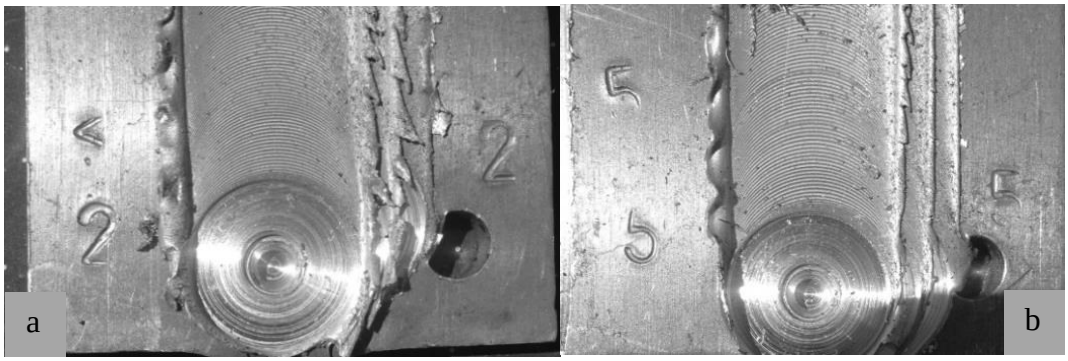

Figure 4.2: Surface of Samples after FSP. Sample (a) number 2 (b) number 5.

4.2 Experiment Results

4.2.1 Energy measurements

Results of energy consumed during process and cost of it are reported in table 4.1.

Table 4.1: Energy measurement results

Sets	N(Rpm)	f (mm/min)	watt	W(Kwh)	Cost(TL)
1	500	63	23812.14	0.338006	0.155483
2	500	160	24782.07	0.164229	0.075546
3	500	250	24132.11	0.115392	0.05308
4	710	250	24580.65	0.122219	0.056221
5	1000	63	24287.28	0.348224	0.160183
6	1000	160	24558.25	0.161735	0.074398
7	1400	63	25593.53	0.359843	0.165528
8	1400	100	25721.39	0.247245	0.113733

Maximum value for energy consumed belongs to set number 7 and minimum value belongs to the set number 3.

4.2.2 Micro-hardness results

Figure 4.3 Shows the results of micro-hardness versus distance from center of the workpiece diagrams of FSP samples which have been produced by variuos values of N and f as mentioned before in table 3.3 .

`

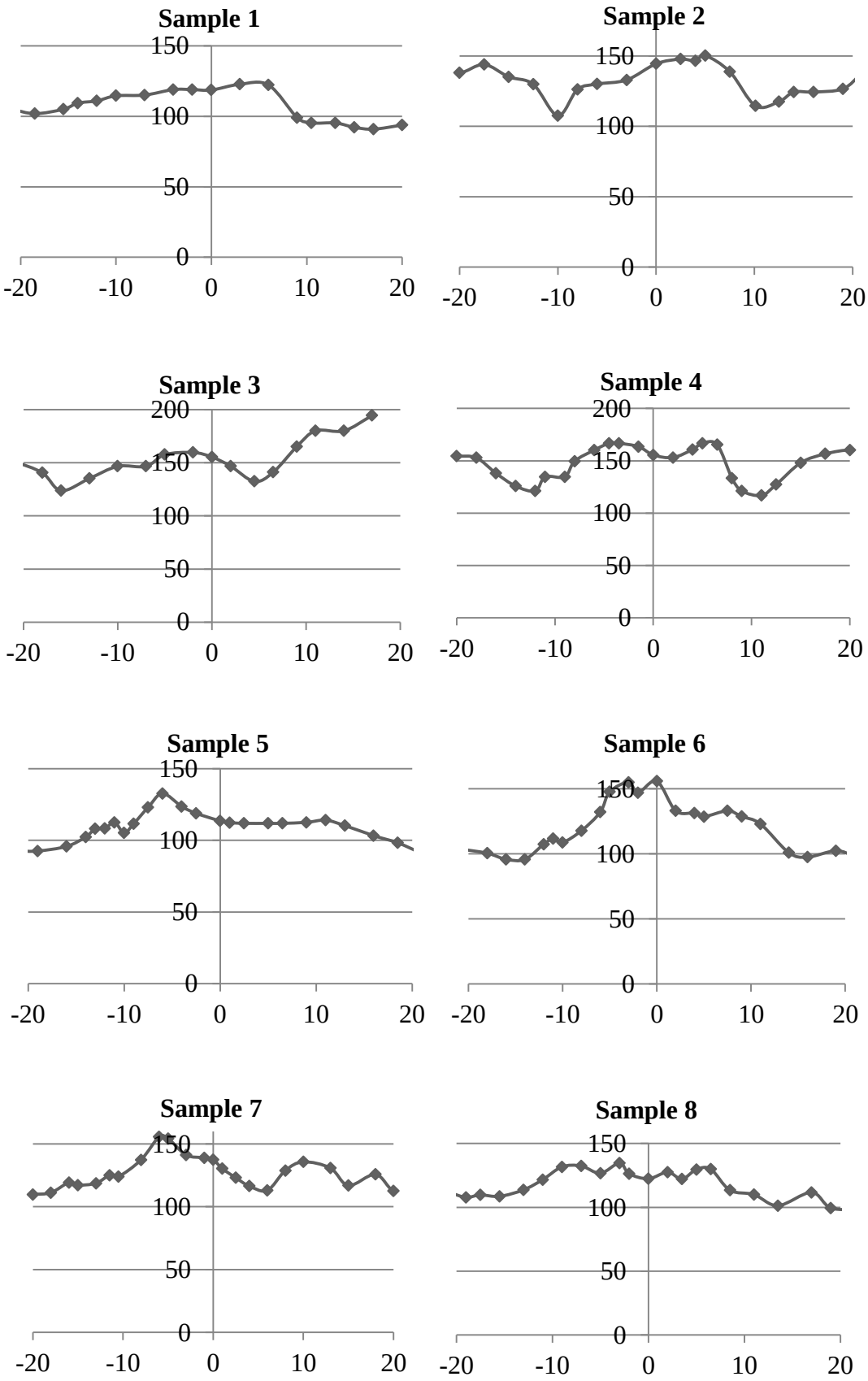

Figure 4.3: Diagrams of micro-hardness Hv10 (Y-axis) versus distance in mm from center of the samples (X-axis).

`

Hardness values of the FSP samples were measured from the TMAZ and HAZ areas. Figure 4.4 shows the Mean Hardness of sample, the best value belongs to the set number 3 (N: 500, f: 250), and the lowest value belongs to the number 5 (N: 1000, f: 63).

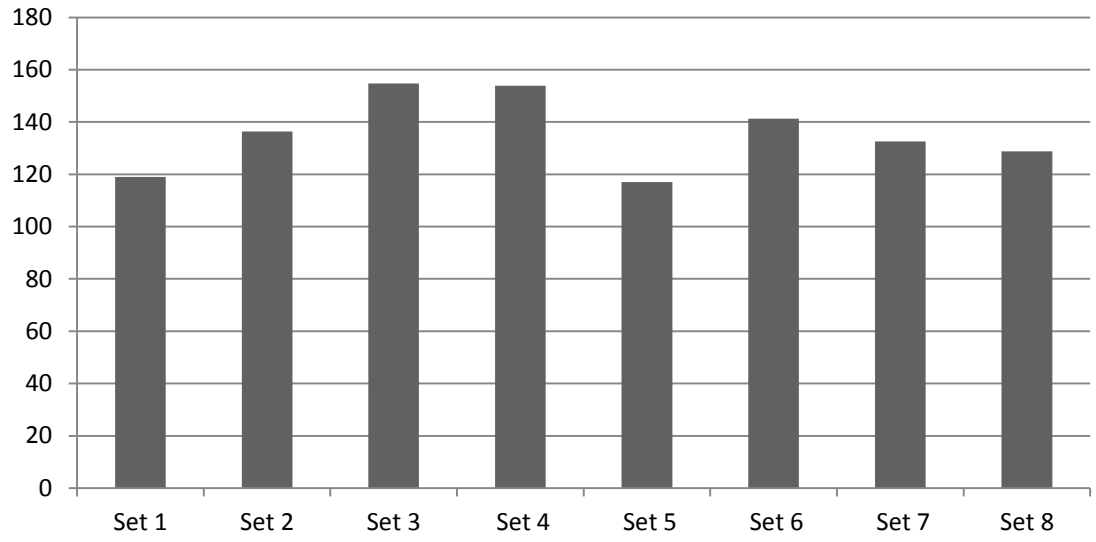

Figure 4.4: Mean Hardness of Samples

4.2.3 Tensile Test Results

By running tensile test, each specimen fractures at specific value of time, force and displacement. Figure 4.5 shows the Stress-Strain curves(x-Strain, y-Stress) of samples, obtained from tensile test; these data's are used to calculate the amount of elongation (mm) and Ultimate Tensile Strength (UTS). Figure 4.6 shows the tensile test samples after fracture.

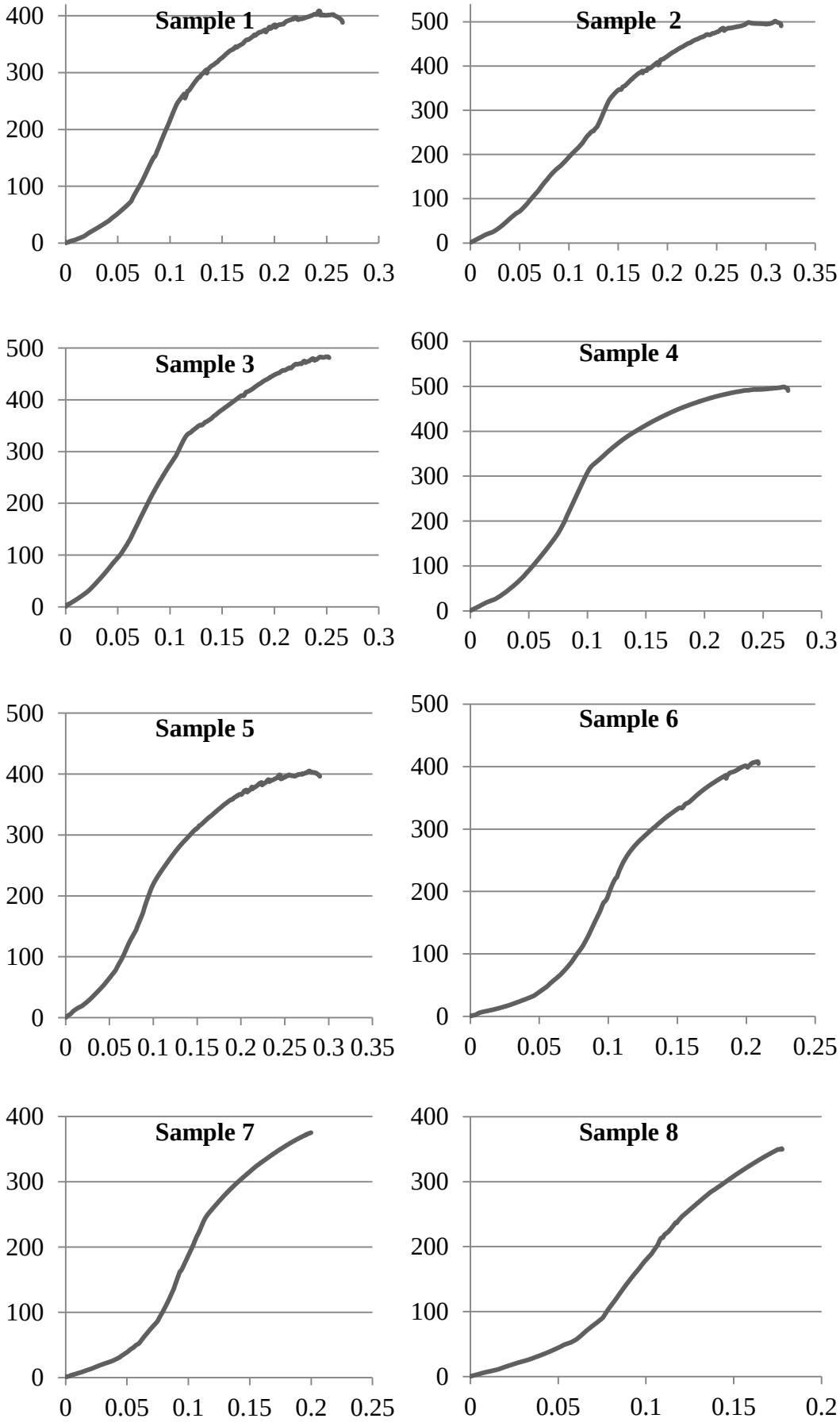

Figure 4.5: Stress (Y-axis) Strain (X-axis) curves obtained from tensile tests.

`

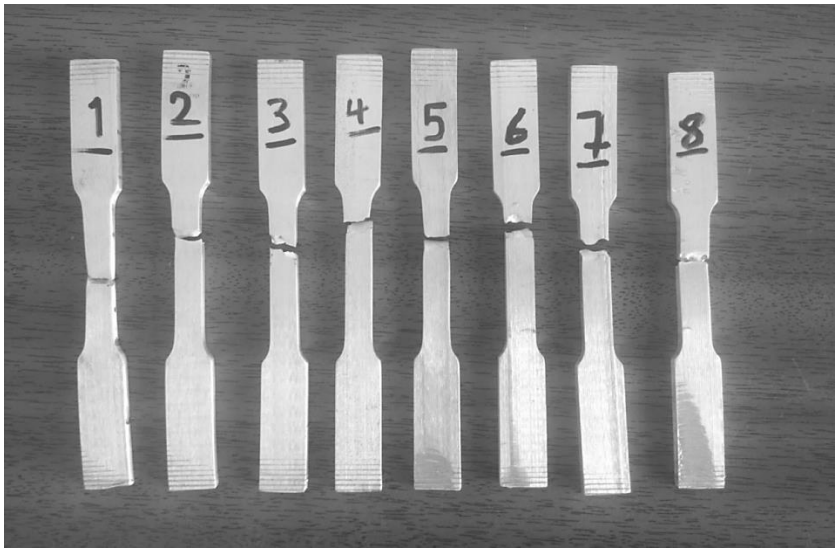

Figure 4.6: Tensile test samples after fracture.

4.3 Discussion

In Table 4.2, the experimental results for elongation, ultimate strength, hardness and cost of consumed electrical energy with respect to various spindle rotational speeds and feed rates are shown.

Table 4.2: Experimental data measured after FSP of test samples

N (rpm)	f (mm/min)	Elongation (mm)	UTS (MPa)	Hardness(HV)	Cost (TL)
500	63	9.86	408.52589	118.92	0.15210
500	160	12.58	501.41520	136.32	0.07390
500	250	9.22	483.36098	154.775	0.05192
710	250	10.17	498.58703	153.8556	0.05499
1000	63	11.15	405.22375	117.0111	0.15670
1000	160	7.21	408.09557	141.2286	0.07278
1400	63	6.83	375.14824	132.5875	0.16192
1400	100	5.95	350.99817	128.8143	0.11126

The experimental results for elongation (mm), ultimate strength, hardness and cost of consumed electrical energy with respect to various spindle rotational speeds and feed rates are shown in Fig. 3 and Fig. 4. The cost of one kwh consumed electrical energy is considered to be 0.5 Turkish Lira (0.25 $) as the reference.

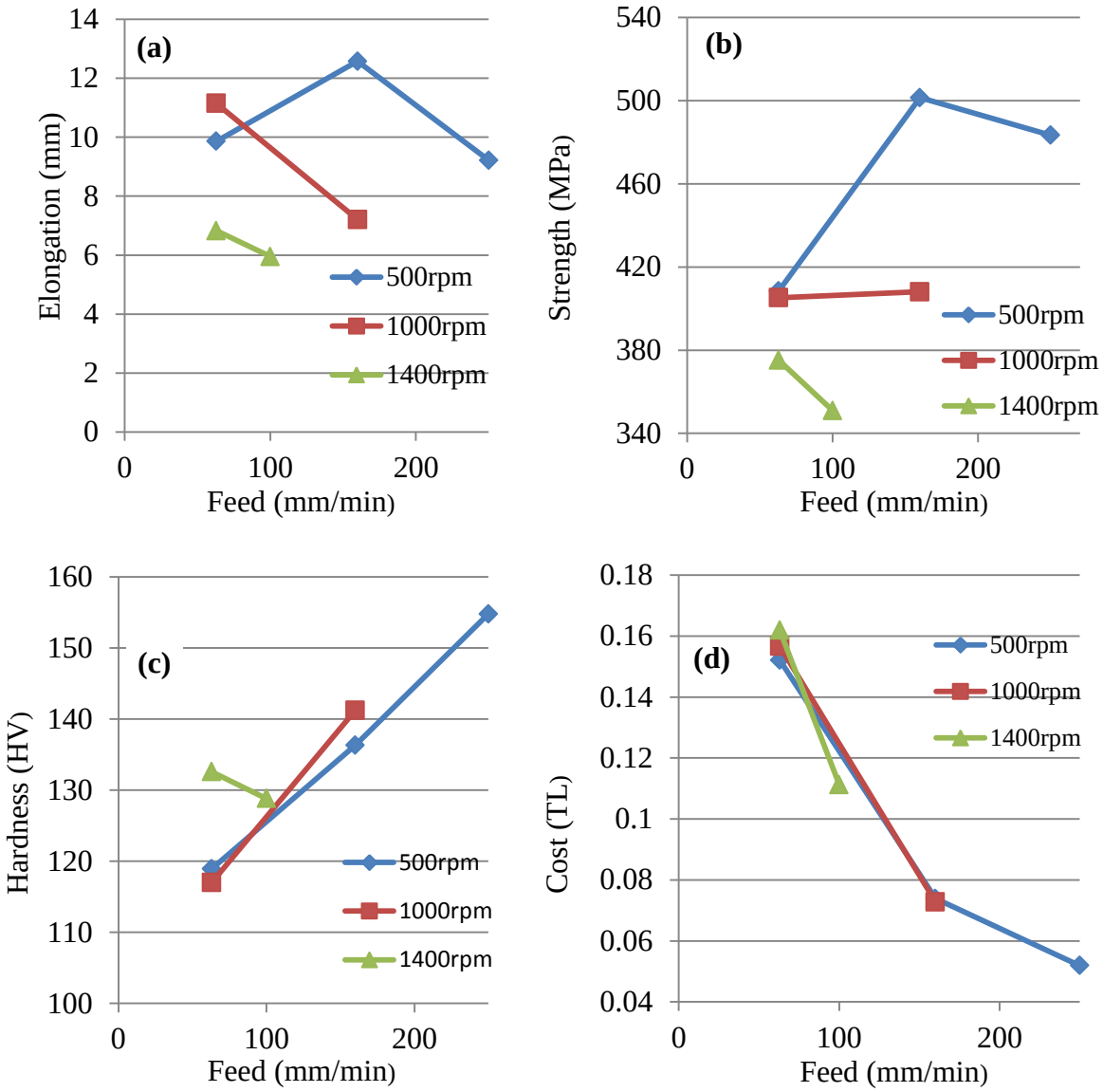

Figure 4.7: Effect of variation in feed on FSP performance measures: (a) Elongation, (b) Strength, (c) Hardness, and (d) Energy cost.

For the fixed rotational speed of 500rpm, the elongation increases (from 9.86 mm to 12.58 mm) as the feed increases from 63mm/min to 160mm/min and decreases afterwards from 160mm/min to 250mm/min (Fig. 4.7(a)). The same is true for ultimate strength (Fig. 4.7(b)). However, the hardness gradually increases while the energy consumption contrarily decreases over the entire range of feed (Figs. 4.7(c) and 4.7(d)). For the fixed speed of 1000rpm and 1400rpm, the trends for elongation are entirely opposite in the invetsigated range of feed. At a fixed speed of 1000rpm,

both the strength and hardness are increased but will be reduced when the speed is increased to 1400rpm. This is to be noticed that the cost, regardless of rotational speed, is decreased as the feed is increased.

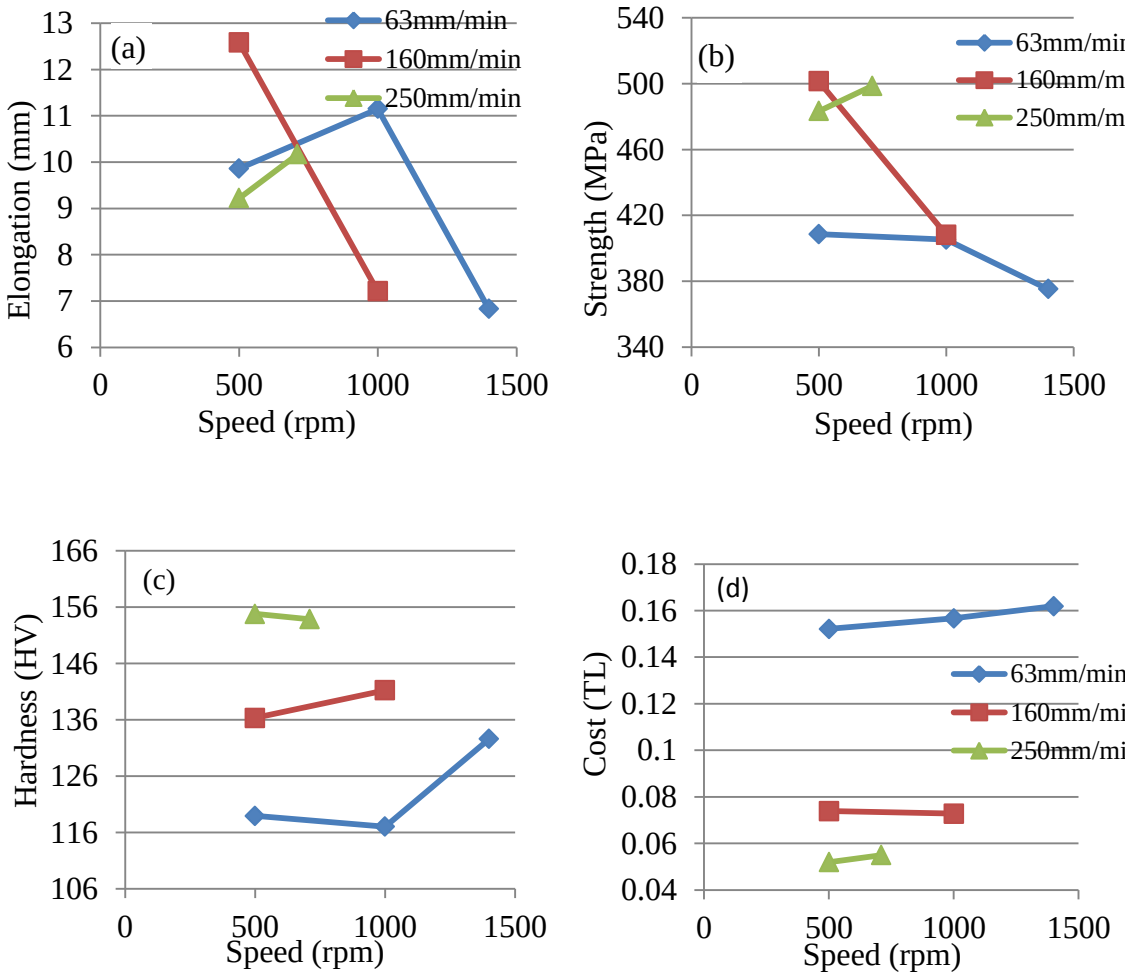

Figure 4.8: Effect of variation in speed on FSP performance measures.

At a constant feed of 63mm/min, the elongation is increased to a certain value (from 9.86 mm to 11.15 mm) as speed is increased from 500rpm to 1000rpm and afterwards (i.e., from 1000rpm to 1400rpm) begins to decrease (Fig. 4.8(a)) . On the other hand, ultimate strength gradually is decreased with the increasing of spindle speed over entire range (Fig. 4.8(b)). However, an increase in the speed causes positive effect on hardness after 1000rpm (Fig. 4.8(c)). The energy consumption also

`

is decerased because the deformation force is decerased at increased speed (Fig. 4.8(d)). This is to be noticed that with 160mm/min feed, the elongation contrary to 63mm/min feed is decreased with the increasing of roational speed from 500rpm to 1000rpm. But, again in agreement with 63mm/min, the elongation is increased with increasing the speed at 250mm/min feed. The same is applicable to strength but not to hardness. On high feeds (160mm/min and 250mm/min), the effect of increasing speed on energy consumption is not so significant.

El-Rayes and El-Danaf [17] for Al6082-T651 found that increasing the feed from 90mm/min to 240mm/min increase strength and hardness, which from strength perspective is in partial agreement with the current study. The effect of rotational speed, in complete contradiction to present study, was found to be insignificant in the range of 850rpm to 1350rpm. For casted Al2285, Karthikeyan et al. [18] observed the elongation and strength to be decreasing and hardness increasing as the feed was increased from 10mm/min to 15mm/min; these trends are in partial agreement with the current work. All of the three quantities, partially contradictory to the current findings, were found to increase with increasing speed from 1400rpm to 1800rpm. Azizieh et al. [24] found that the hardness of AZ31/Al_2O_3 decreased with increasing the speed from 800rpm to 1200rpm, while Zohoori et al. [26] reported that both the hardness and strength are increased as the rotational speed is increased from 700rpm to 1900rpm. From the above results, it follows that the effects of variation in parameters on various mechanical properties is extremely interactive and non-linear. In other words, the effects are coupled with the settings of the parameters. These parameter-coupled variations in the properties of Al7075 can be attributed to the phase/microstructure changes caused by the FSP thermal cycles. Further, the comparison between the current and previous studies reveals that the effects of FSP

`

parameters are not unique rather their nature depends on the type of material employed.

Figure 4.9 presents the measured experimental data in three dimensional views.

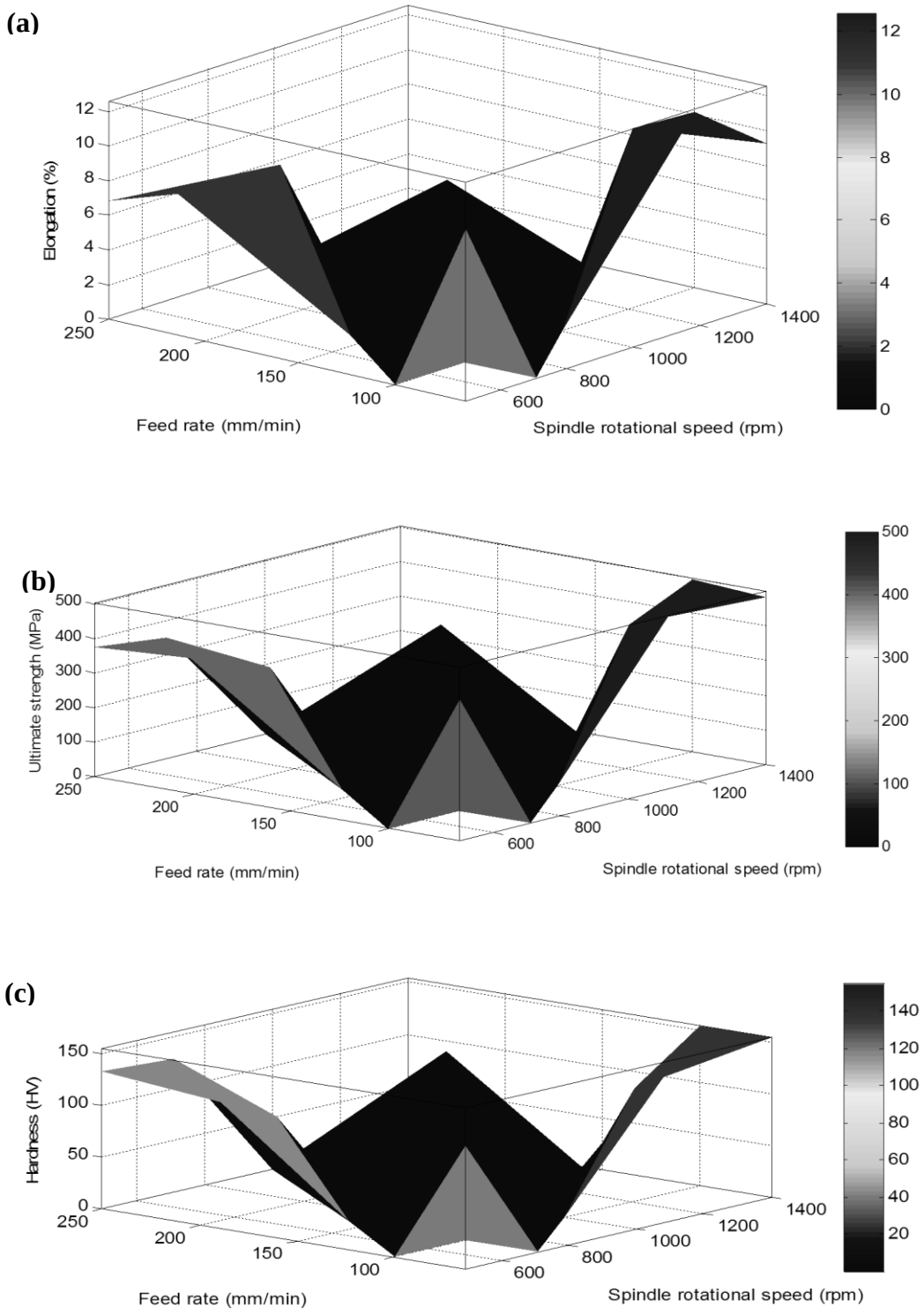

`

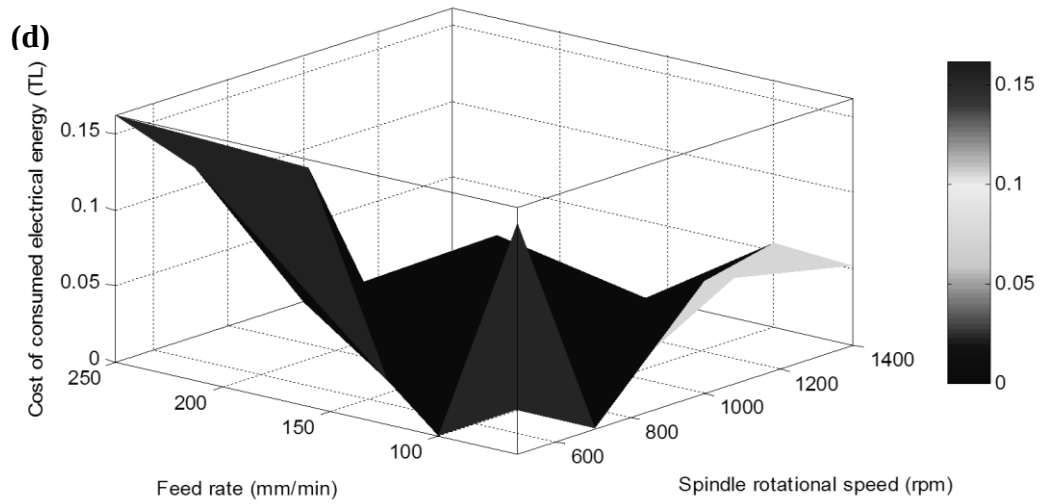

Figure 4.9: Presentation of measured experimental data in three dimensional view: (a) Elongation, (b) Ultimate tensile strength, (c) Hardness, and (d) Energy cost.

Figure 4.10 depicts the optimum results of ANN modeling of FSP when cases "a-d" are with 3 layers, each layer contains 50 Neurons, and with 5 Epochs. Also, in Fig. 10, cases "e-h" show the optimum simulation results with ANN configuration of 2 layers, each layer contains 35 Neurons, with 5 Epochs. Also, it indicates that with increment of number of layers and number of neurons, the approximated values of all objective functions except elongation, is increased. Moreover, the general trend of approximated results by various ANNs configuration with respect to speed feed and spindle speed is very similar with each other.

However, the maximum and minimum of approximated values for ultimate strength and hardness by various ANN configurations are located on various locations of design space. The approximation results from various ANN configurations show the nonlinear behavior of objective functions, Figure 4.10.

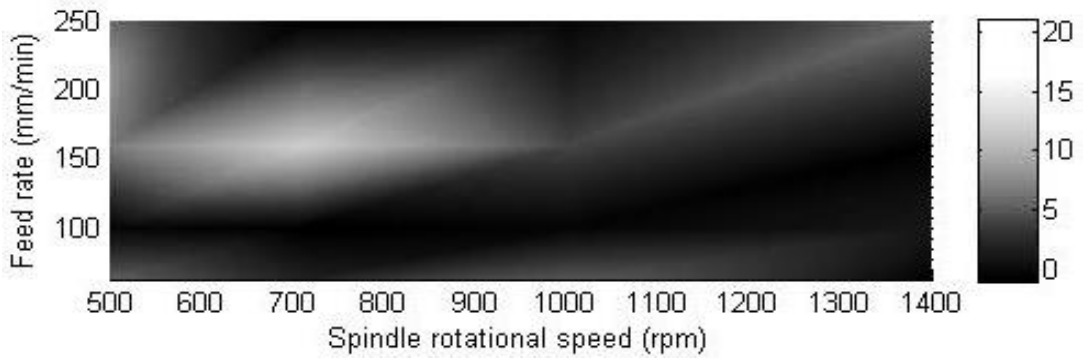

(a) ANN results for Elongations (mm) with 3 layers, each layer contains 50 Neurons, with 5 Epochs

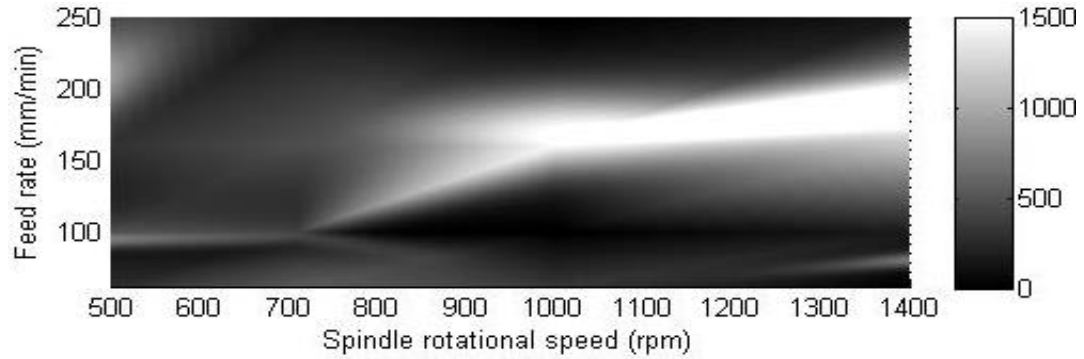

(b) ANN results for Ultimate Strength (MPa) with 3 layers, each layer contains 50 Neurons, with 5 Epochs

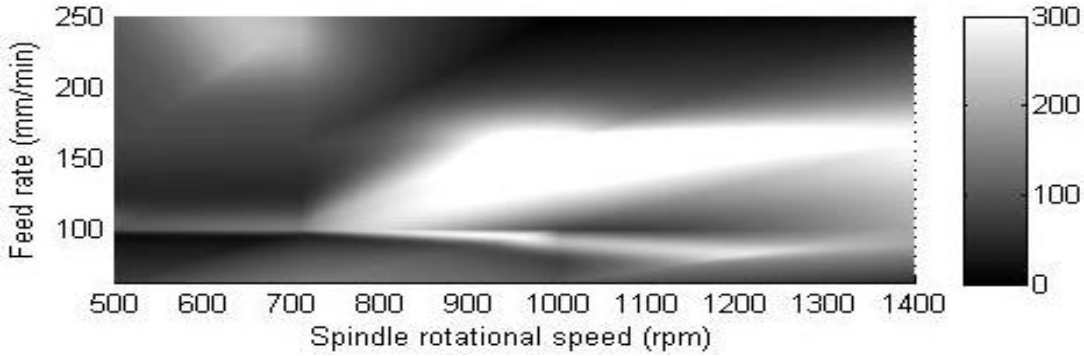

(c) ANN results for Hardness (HV) with 3 layers, each layer contains 50 Neurons, with 5 Epochs

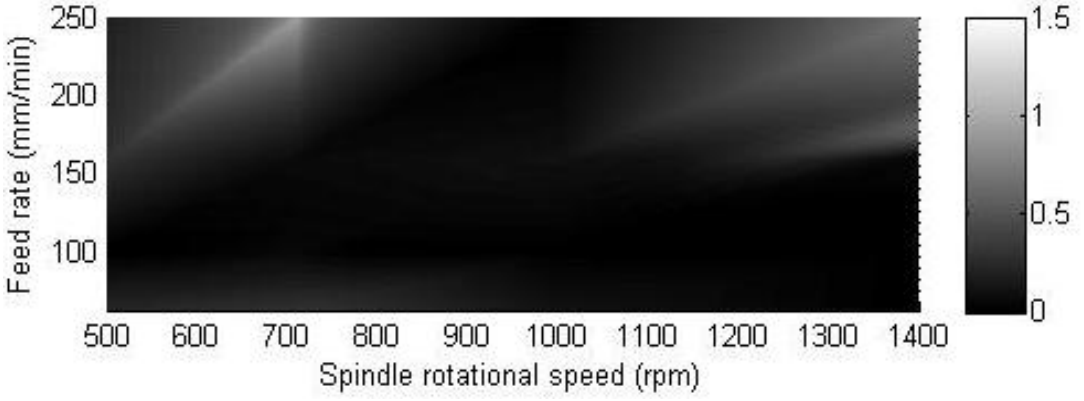

(d) ANN results for Energy consumption cost (in Turkish Lira) with 3 layers, each layer contains 50 Neurons, with 5 Epochs

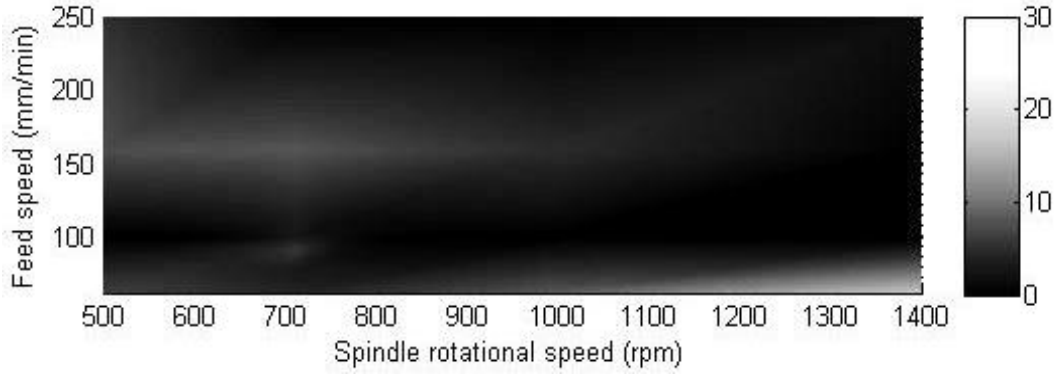

(e) ANN results for Elongations (mm) with 2 layers, each layer contains 35 Neurons, with 5 Epochs

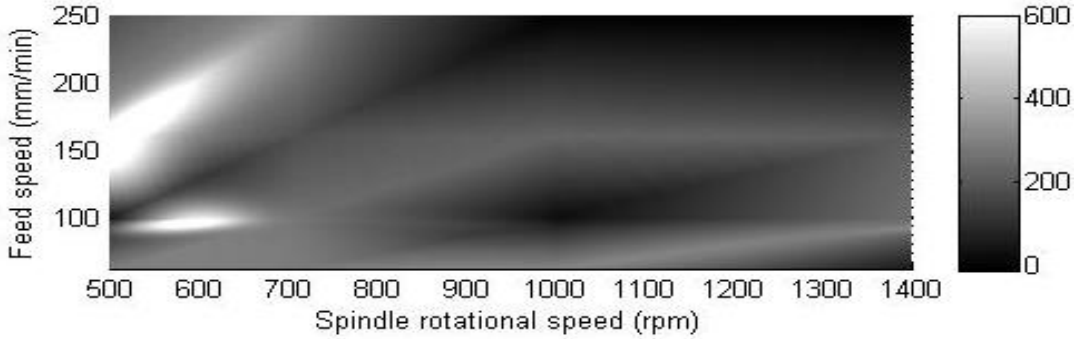

(f) ANN results for Ultimate strength (MPa) with 2 layers, each layer contains 35 Neurons, with 5 Epochs

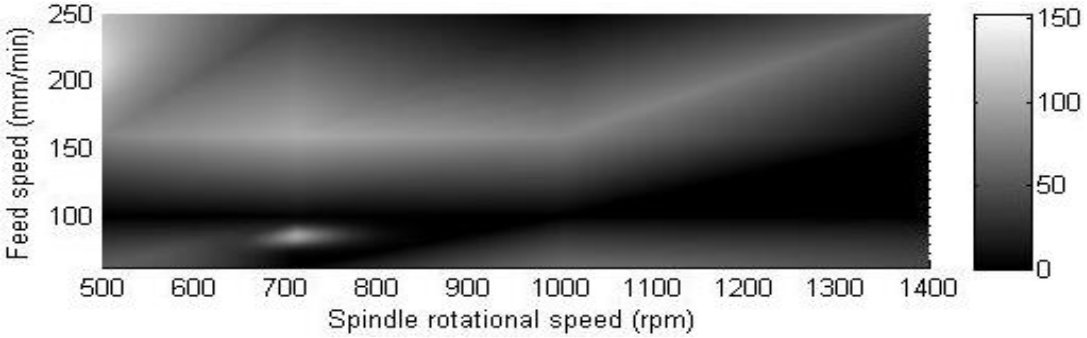

(g) ANN results for hardness (HV) with 2 layers, each layer contains 35 Neurons, with 5 Epochs

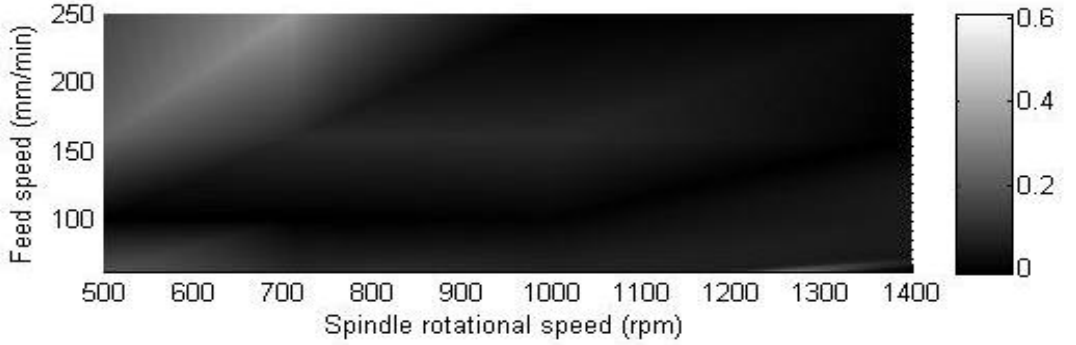

(h) ANN results for Energy consumption cost (in Turkish Lira) with 2 layers, each layer contains 35 Neurons, with 5 Epochs

Figure 4.10: Results of ANN modeling of FSP.

`

Tables 4.3 and 4.4 show the optimization resluts and their experimental verification when various ANN structures are used. In Table 4.3, the optimum simulation results from an ANN with 3 layers, 50 neurons in each layer and maximum 5 epochs are compared with the experimental results. Also, in Table 4.4, the same procedure is repeated with ANN which has 2 layers, 35 neurons in each layer and maximum epochs of 5.

Table 4.3: Optimum results of ANN-based multiobjective genetic optimization with 3 layers, 50 neurons in each layer, maximum number of epochs of 5 and their experimental verifications.

Type of measurement	N (rpm)	f (mm/min)	Elongation (mm)	UTS (MPa)	Hardness (HV)	Cost (TL)
Simulation	700	160	19.35	537.38	131.64	0.14
Experimental			21.37	526.49	127.31	0.17

Table 4.4: Optimum results of ANN-based multiobjective genetic optimization with 2 layers, 35 neurons in each layer, maximum number of epochs of 5 and their experimental verifications.

Type of measurement	N (rpm)	f (mm/min)	Elongation (mm)	UTS (MPa)	Hardness (HV)	Cost (TL)
Simulation	500	160	12.36	180.47	84.51	0.17
Experimental			11.68	175.38	87.32	0.21

In order to verify the optimization results, tests were conducted both for 3 layers and 2 layers. As can be seen from Tables 2 and 3, the empirical results are in good compromise with the predicted ones. Therefore, it can be said that ANN can be successfully employed to predict and optimize FSP. From the tables, it is to be observed that the best results are offered when FSP is performed with rotational speed of 160mm/min and 700rpm.

`

Chapter 5

CONCLUSION

The effects of spindle speed and feed of FSP on various mechanical properties of Al7075 and energy consumption were examined in this study. It was found that the effects were quite interactive and closely linked with the opted magnitude of the parameters. As instance, with the fixed rotational speed of 500rpm, the elongation was increased (from 9.86 mm to 12.58 mm) to a certain range of feed (i.e., from 63mm/min to 160mm/min) and was decreased afterwards (i.e., from 160mm/min to 250mm/min). The same was found to be true for ultimate strength. The hardness, on the contrary, gradually was increased and the energy consumption contrarily was decreasesd over the entire range of feed. In summary, the effects of FSP parameters were found to be highly intercative, non-linear as well opposing in nature on various performance measures of FSP.

To find a trade-off among various mechanical properties of Al7075 and energy consumed while processing, ANN with GA was employed. The best parameters that offered high mechanical properties of Al7075 and low energy cost/consumption were found to be as follows: feed speed=700 (mm/min) and rotational speed=160 (rpm).

This study has demonstrated that ANN coupled with GA can be used as a powerful tool for multi-objective decision modeling and optimization in FSP.

`

The findings reported herein work will act as a guideline for the users of FSP, following which one can easily find the optimal parameters for the other materials of interest as well.

`

REFERENCES

[1] Campbell Jr, F.C. (2011). Manufacturing technology for aerospace structural materials. *Elsevier.*

[2] Charit, I., & Mishra R.S. (2003). High strain rate superplasticity in a commercial 2024 Al alloy via friction stir processing. *Materials Science and Engineering*. *A 359*, 290-296.

[3] Thomas, W.M., Nicholas, E.D., Needham, J.C., Murch, M.G., Temple-Smith, P., & Dawes, C.J. (1991). International Patent Application PCT/GB92/02203 and GB Patent Application 9125978. *UK Patent Office*. London.

[4] Nicholas, ED. (1998). Developments in the friction stir welding of metals. ICAA-6. 6th International Conference on Aluminum Alloys. Japan.

[5] Mishra, R.S., Mahoney, M.W., McFadden, S.X., Mara, N.A., Mukherjee, A.K. (2000). *Scripta Mater*. *42*, 163.

[6] Mishra, R.S., Mahoney, M.W. (2001). *Material Science.* Forum 357-359.

[7] Haykin, S. (2009). Neural Networks and Learning Machines. *Prentice Hall*. Volume 10.

[8] Ma, Z.Y., Mishra, R.S., Mahoney, M.W. (2002). *Acta Mater*. *50*, 4419.

`

[9] Mahoney, M.W., Mishra, R.S., Nelson, T., Flintoff, J., Islamgaliev, R., & Hovansky, Y. (2001). High strain rate, Thick section superplasticity created via friction stir processing. *Friction Stir welding and Processing.* 183- 194.

[10] Mishra, R.S., Ma, Z.Y., Charit, I. (2002). *Material Science*. Eng. A 341, 307.

[11] Ma, Z.Y., Sharma, S.R., Mishra, R.S., Mahoney, M.W. (2003). *Material Science*. Forum 426–432.

[12] Hsu, C.J., et al. (2006). Al-Al3Ti nanocomposites produced in situ by friction stir processing. *Acta Materialia*. 5241-5249.

[13] Mishra, R.S., Ma, Z.Y., Charit, I. (2005). Friction Stir Welding And Processing. *Material Science and Engineering*. *R 50*, 1-78.

[14] Cavaliere, P., De Marco, P.P. (2007). Fatigue behaviour of friction stir processed AZ91 magnesium alloy produced by high pressure die casting. *Materials Characterization*. *58(3)*, 226-232.

[15] Commin, L., et al. (2009). Friction stir welding of AZ31 magnesium alloy rolled sheets: Influence of processing parameters. *Acta Materialia*. *57(2)*, 326-334.

[16] Abbasi Gharacheh, M., et al. (2006). The influence of the ratio of "rotational speed/traverse speed" (ω/v) on mechanical properties of AZ31 friction stir welds. *International Journal of Machine Tools and Manufacture*. *46(15).*

`

[17] El-Rayes, M.M., & El-Danaf, E.A. (2012). The influence of multi-pass friction stir processing on the microstructural and mechanical properties of Aluminum Alloy 6082. *Journal of Materials Processing Technology*. *212(5),* 1157-1168.

[18] Karthikeyan, L., et al. (2009). Mechanical property and microstructural changes during friction stir processing of cast aluminum 2285 alloy. *Materials and Design*. *30(6),* 2237-2242.

[19] Karthikeyan, L., Senthilkumar, V.S., & Padmanabhan, K.A. (2010). On the role of process variables in the friction stir processing of cast aluminum A319 alloy. *Materials and Design*. *31(2),* 761-771.

[20] Ma, Z.Y., Sharma, S.R., & Mishra, R.S. (2006). Effect of friction stir processing on the microstructure of cast A356 aluminum. *Materials Science and Engineering*. *433(1-2),* 269-278.

[21] Ma, Z.Y., Sharma, S.R., & Mishra, R.S. (2006). Effect of multiple-pass friction stir processing on microstructure and tensile properties of a cast aluminum–silicon alloy. *Scripta Materialia*. *54(9),* 1623-1626.

[22] Johannes, L.B., & Mishra, R.S. (2007). Multiple passes of friction stir processing for the creation of superplastic 7075 aluminum. *Materials Science and Engineering*. *464(1–2),* 255-260.

[23] Bauri, R., Yadav, D., & Suhas, G. (2011). Effect of friction stir processing (FSP) on microstructure and properties of Al–TiC in situ composite. *Materials*

`

Science and Engineering. 528(13–14), 4732-4739.

[24] Azizieh, M., Kokabi, A.H., & Abachi, P. (2011). Effect of rotational speed and probe profile on microstructure and hardness of AZ31/Al2O3 nanocomposites fabricated by friction stir processing. *Materials & Design. 32(4),* 2034-2041.

[25] Faraji, G., & Asadi, P. (2011). Characterization of AZ91/alumina nanocomposite produced by FSP. *Materials Science and Engineering*. *528(6),* 2431-2440.

[26] Zohoor, M., Besharati, M.K., & Salami, P. (2012). Effect of processing parameters on fabrication of Al–Mg/Cu composites via friction stir processing. *Materials & Design*. *39,* 358-365.

[27] Thomas, W.M., Nicholas, E.D., & Kallee, S.W. (2001). Friction based technologies for joining and processing. *Friction Stir Welding and Processing*. 3-13.

[28] Sharifitabar, M., et al. (2011). Fabrication of 5052Al/Al2O3 nanoceramic particle reinforced composite via friction stir processing route. *Materials & Design*. *32(8–9),* 4164-4172.

[29] Bahrami, M., et al. (2014). On the role of pin geometry in microstructure and mechanical properties of AA7075/SiC nano-composite fabricated by friction stir welding technique. *Materials & Design*. *53(0),* 519-527.

`

[30] Elangovan, K., & Balasubramanian, V. (2008). Influences of tool pin profile and tool shoulder diameter on the formation of friction stir processing zone in AA6061 aluminium alloy. *Materials & Design*. *29(2)*, 362-373.

[31] McCulloch, W., & Pitts, W. (1943). A logical calculus of the ideas immanent in nervous activity. *The bulletin of mathematical biophysics*. *5(4)*, 115-133.

[32] Hebb, Donald. (1949). The Organization of Behavior. *Wiley*. New York.

[33] Rosenblatt, F. (1958). The Perceptron: A Probalistic Model For Information Storage And Organization In The Brain. *Psychological Review*. *65*, 386–408.

[34] Werbos, P.J. (1975). Beyond Regression: New Tools for Prediction and Analysis in the Behavioral Sciences.

[35] Russell, Ingrid. (2012). Neural Networks Module.

[36] Yang, J.J., Pickett, M.D., Li, X.M., Ohlberg, D.A., Stewart, D.R., Williams, R.S. (2008). *Nanotechnol*. *3*, 429–433.

[37] Strukov, D.B., Snider, G.S., Stewart, D.R., Williams, R.S. (2008). *Nanotechnol*. *453*, 80–83.

[38] Arslan, M.A., Hajela, P. (2001). Use of Counter propagation neural networks to enhance the concurrent subspace optimization strategy. *Engineering Optimization*. *33*, 327–349.

`

[39] Papadrakakis, M., Lagaros, N.D., Tsompanakis, Y. (1999). Optimization of large-scale 3-D trusses using evolution strategies and neural networks. *International Journal of Structural Integrity*. *14*, 211–223.

[40] Ranjbar, M., Marburg, S. (2013). Fast vibroacoustic optimization of mechanical structures using artificial neural networks. *International Journal of Mechanical Sciences*. *1–3*, 64–68.

[41] Goldberg, D.E. (1989). Genetic algorithms in search, optimization, and machine learning, *Addison-Wesley*.

[42] Podlena, J., Hendtlass, T. (1998). An accelerated genetic algorithm, *Applied Intelligence*. *8(2)*, 103-111.

[43] Kalyanmoy, D. (2001). Multi-Objective Optimization using Evolutionary Algorithms, *John Wiley & Sons*.

[44] Hong, T., Wang, H., Lin, W., & Lee, W. (2002). Evolution of appropriate crossover and mutation operators in a genetic process, *Applied Intelligence*. *16*, 7-17.

[45] Porwal, R.K., Yadava, V., & Ramkumar, J. (2012). Artificial neural network modelling and multi objective optimisation of hole drilling electro discharge micro machining of invar. *International Journal of Mechatronics and Manufacturing Systems*. *5*(5), 470–494.

[46] Xie, D., et al. (2012). Modeling of CNC machine tool energy consumption and optimization study based on neural network and genetic algorithm. *Applied Mechanics and Materials*. 770-776.

[47] Xiong, J., Zhang, G., Hu, J., Wu, L. (2012). Bead geometry prediction for robotic GMAW-based rapid manufacturing through a neural network and a second-order regression analysis. *Journal of Intelligent Manufacturing*. 1–7.

[48] Tansel, I., et al. (2010). Optimizations of friction stir welding of aluminum alloy by using genetically optimized neural network. *The International Journal of Advanced Manufacturing Technology*. ***48****(1-4)*, 95-101.

[49] Shojaeefard, M.H., et al. (2013). Modelling and Pareto optimization of mechanical properties of friction stir welded AA7075/AA5083 butt joints using neural network and particle swarm algorithm. *Materials & Design*. 190-198.

[50] Hussain, G., Gao, L., Hayat, N. (2009). Empirical modelling of the influence of operating parameters on the spifability of a titanium sheet using response surface methodology. *Proc IMechE J Engrg Manuf. 223*, 73–81.

[51] Wong, S.V., Hamouda, A.M.S., and El Baradie, M.A. (1999). Generalized fuzzy model for metal cutting data selection. *Journal of Materials Processing Technology*. *89–90(0)*, 310-317.

[52] Metals Handbook, Volume 2. (1990). Properties and Selection: Nonferrous Alloys and Special-Purpose Materials. *ASM International* 10th Edition.

`

[53] Book of Standards Volume: 03.01. ASTM E8-13a,Standard Test Methods for Tension Testing of Metallic Materials. Active Standard ASTM E8.

[54] Zitzler, E., Laumanns, M., & Bleuler, S. (2004). A Tutorial on Evolutionary Multiobjective Optimization, in Metaheuristics for Multiobjective Optimisation. *Springer Berlin Heidelberg*. 3-37.

[55] Hultmann Ayala, H.V., Santos Coelho, L. (2007). A Multiobjective Genetic Algorithm Applied to Multivariable Control Optimization. *19th International Congress of Mechanical Engineering*. Brasília, DF.

[56] Ranjbar, M. (2010). A Comparative Study on Optimization in Structural Acoustics. Ph.D. Thesis. Department of Mechanical Engineering, Technische Universitaet Dresden, Germany.

[57] Canadian Standards Association, Energy Efficiency Test Methods for Three-phase Motors, Performance of Electrical Products, ISSN 0317·5669 Published in July 1993, Ontario, Canada.

`

APPENDIX

`

Appendix A: Artificial Neural Network Modelling

```
%Artificial Neural Network Modelling
clc
clear all
%Spindle Speeds
input(1,1)= 500;
input(1,2)= 710;
input(1,3)= 1000;
input(1,4)= 1400;

%Feed Rates
input(2,1)= 63;
input(2,2)= 100;
input(2,3)= 160;
input(2,4)= 250;

%Elongation
S(1,1)= 9.86;
S(1,3)= 12.58;
S(1,4)= 9.22;
S(2,4)= 10.17;
S(3,1)= 11.15;
S(3,3)= 7.21;
S(4,1)= 6.83;
S(4,2)= 5.95;

%Ultimate Strength
S1(1,1)= 408.52589;
S1(1,3)= 501.4152072;
S1(1,4)= 483.3609847;
S1(2,4)= 498.5870329;
S1(3,1)= 405.223754;
S1(3,3)= 408.0955743;
S1(4,1)= 375.1482436;
S1(4,2)= 350.9981734;

%Hardness
S2(1,1)= 118.92;
S2(1,3)= 136.32;
S2(1,4)= 154.775;
S2(2,4)= 153.8556;
S2(3,1)= 117.0111;
S2(3,3)= 141.2286;
S2(4,1)= 132.5875;
S2(4,2)= 128.8143;

%Power Consumptio
S3(1,1)= 0.338005656;
S3(1,3)= 0.164229395;
```

`

```
S3(1,4)= 0.115391948;
S3(2,4)= 0.122219246;
S3(3,1)= 0.34822381;
S3(3,3)= 0.161734978;
S3(4,1)= 0.359842893;
S3(4,2)= 0.247245174;

input1=input(1,1:end);
input2=input(2,1:end);

%Draw the initial data from Experiments
subplot(4,2,1);
surf(input1,input2,S,'FaceColor','interp','EdgeColor','none','FaceLighting','phong');
title('Elongation-original');
axis tight
view(-50,30)
camlight right

subplot(4,2,3);
surf(input1,input2,S1,'FaceColor','interp','EdgeColor','none','FaceLighting','phong');
title('Ultimate Strength-original');
axis tight
view(-50,30)
camlight right

subplot(4,2,5);
surf(input1,input2,S2,'FaceColor','interp','EdgeColor','none','FaceLighting','phong');
title('Hardness-original');
axis tight
view(-50,30)
camlight right

subplot(4,2,7);
surf(input1,input2,S3,'FaceColor','interp','EdgeColor','none','FaceLighting','phong');
title('Powr Consumption-original');
axis tight
view(-50,30)
camlight right

%-----Feedforward Backpropogation Neural Networks Algorithm------
%-----creating a neural network and training it----------

I=[input1;input2];
net = feedforwardnet;
net.trainParam.epochs =10;
net.trainParam.lr= 0.01;
net.numLayers = 3;
net.layers{1}.size = 2;
net.layers{2}.size = 2;
net.layers{3}.size = 2;
```

`

```
net.biases{1}.learnFcn = 'learnp';
net.divideFcn='divideint';
net.divideParam.trainRatio = 70/100;
net.divideParam.valRatio = 15/100;
net.divideParam.testRatio = 15/100;

net = configure(net,I,S);

net=train(net,I,S);
%view(net);
z=net(I);
perf=perform(net,z,S);

dx1=1;
dy1=1;

x1_edge=[floor(min(input1)):dx1:ceil(max(input1))];
y1_edge=[floor(min(input2)):dy1:ceil(max(input2))];
[X1,Y1]=meshgrid(x1_edge,y1_edge);
Z=griddata(input1,input2,z,X1,Y1);
%F1 = TriScatteredInterp(input1,input2,z);
%Z= F1(X1,Y1);
subplot(4,2,2);

surf(X1,Y1,Z,'FaceColor','interp','EdgeColor','none','FaceLighting','phong');
%surf(input1,input2,z,'FaceColor','interp','EdgeColor','none','FaceLighting','phong');
title('Elongation-NN');
%daspect([5 5 1])
axis tight
view(-50,30)
camlight left

%camlight left; lighting phong;
A=max(max(S));%minimum value of the shubert function
%A=min(min(Z));%minimum value of the approximated initial function
B=max(max(Z));%maximum value of the created network
errors = gsubtract(A,B);

%Train the Ultimate Stength
net1 = configure(net,I,S1);

net1=train(net1,I,S1);
%view(net);
z1=net1(I);
perf1=perform(net1,z1,S1);

subplot(4,2,4);

%surf(X1,Y1,Z1,'FaceColor','interp','EdgeColor','none','FaceLighting','phong');
surf(input1,input2,z1,'FaceColor','interp','EdgeColor','none','FaceLighting','phong');
```

`

```
title('Ultimate Stregth-NN');
%daspect([5 5 1])
axis tight
view(-50,30)
camlight left

%camlight left; lighting phong;
A1=max(max(S1));%minimum value of the shubert function
%A=min(min(Z));%minimum value of the approximated initial function
B1=max(max(z1));%maximum value of the created network
errors1 = gsubtract(A1,B1);

%Train the Hardness
net2 = configure(net,I,S2);

net2=train(net2,I,S2);
%view(net);
z2=net2(I);
perf2=perform(net2,z2,S2);

subplot(4,2,6);

%surf(X1,Y1,Z1,'FaceColor','interp','EdgeColor','none','FaceLighting','phong');
surf(input1,input2,z2,'FaceColor','interp','EdgeColor','none','FaceLighting','phong');
title('Hardness-NN');
%daspect([5 5 1])
axis tight
view(-50,30)
camlight leftz1

); %camlight left; lighting phong;
A2=max(max(S2));%minimum value of the shubert function
%A=min(min(Z));%minimum value of the approximated initial function
B2=max(max(z2));%minimum value of the created network
errors2 = gsubtract(A2,B2);

%Train the Cost of Energy
net3 = configure(net,I,S3);

net3=train(net3,I,S3);
%view(net);
z3=net3(I);
perf3=perform(net3,z3,S3

subplot(4,2,8);

%surf(X1,Y1,Z1,'FaceColor','interp','EdgeColor','none','FaceLighting','phong');
surf(input1,input2,z3,'FaceColor','interp','EdgeColor','none','FaceLighting','phong');
title('Power Consumption-NN');
%daspect([5 5 1])
```

`

```
axis tight
view(-50,30)
camlight left

%camlight left; lighting phong;
A3=min(min(S3));%minimum value of the shubert function
%A=min(min(Z));%minimum value of the approximated initial function
B3=min(min(z3));%minimum value of the created network
errors3 = gsubtract(A3,B3);
```

`

Appendix B: Multiobjective Genetic Algorithm (gamultiobj)

```
% Performing a Multiobjective Optimization Using the Genetic Algorithm
% This example shows how to perform a multiobjective optimization
% using multiobjective genetic algorithm function |gamultiobj| in
% Global Optimization Toolbox.

%   Copyright 2007-2012 The MathWorks, Inc.

%% Simple Multiobjective Optimization Problem
% |gamultiobj| can be used to solve multiobjective optimization problem in
% several variables. Here we want to minimize two objectives, each having
% one decision variable.

%     min F(x) = [objective1(x); objective2(x)]
%      x
%     where, objective1(x) = (x+2)^2 - 10, and
%           objective2(x) = (x-2)^2 + 20
% Plot two objective functions on the same axis
x = -10:0.5:10;
f1 = (x+2).^2 - 10;
f2 = (x-2).^2 + 20;
plot(x,f1);
hold on;
plot(x,f2,'r');
grid on;
title('Plot of objectives "(x+2)^2 - 10" and "(x-2)^2 + 20"');
% The two objectives have their minima at x = -2 and x = +2 respectively.
% However, in a multiobjective problem, x = -2, x = 2, and any solution in
% the range -2 <= x <= 2 is equally optimal. There is no single solution to
% this multiobjective problem. The goal of the multiobjective genetic
% algorithm is to find a set of solutions in that range (ideally with a
% good spread). The set of solutions is also known as a Pareto front. All
% solutions on the Pareto front are optimal.

%%  Coding the Fitness Function
% We create a MATLAB-file named simple_multiobjective.m:
%     function y = simple_multiobjective(x)
%     y(1) = (x+2)^2 - 10;
%     y(2) = (x-2)^2 + 20;
% The Genetic Algorithm solver assumes the fitness function will take one
% input x, where x is a row vector with as many elements as the number of
% variables in the problem. The fitness function computes the value of
% each objective function and returns these values in a single vector
% output y.
%% Minimizing Using |gamultiobj|
% To use the |gamultiobj| function, we need to provide at least two input
% arguments, a fitness function, and the number of variables in the problem.
% The first two output arguments returned by |gamultiobj| are X, the points
% on Pareto front, and FVAL, the objective function values at the values X.
```

`

```
% A third output argument, exitFlag, tells you the reason why |gamultiobj|
% stopped. A fourth argument, OUTPUT, contains information about the
% performance of the solver. |gamultiobj| can also return a fifth argument,
% POPULATION, that contains the population when |gamultiobj| terminated and a
% sixth argument, SCORE, that contains the function values of all
% objectives for POPULATION when |gamultiobj| terminated.
FitnessFunction = @simple_multiobjective;
numberOfVariables = 1;
[x,fval] = gamultiobj(FitnessFunction,numberOfVariables);

% The X returned by the solver is a matrix in which each row is the
% point on the Pareto front for the objective functions. The FVAL is a
% matrix in which each row contains the value of the objective functions
% evaluated at the corresponding point in X.
size(x)
size(fval)

% Constrained Multiobjective Optimization Problem
% |gamultiobj| can handle optimization problems with linear inequality,
% equality, and simple bound constraints. Here we want to add bound
% constraints on simple multiobjective problem solved previously.
%
%    min F(x) = [objective1(x); objective2(x)]
%    x
%    subject to  -1.5 <= x <= 0 (bound constraints)
%
%    where, objective1(x) = (x+2)^2 - 10, and
%          objective2(x) = (x-2)^2 + 20
%
% |gamultiobj| accepts linear inequality constraints in the form A*x <= b and
% linear equality constraints in the form Aeq*x = beq and bound constraints
% in the form lb < x < ub. We pass A and Aeq as matrices and b, beq, lb,
% and ub as vectors. Since we have no linear constraints in this example, we
% pass [] for those inputs.
A = []; b = [];
Aeq = []; beq = [];
lb = -1.5;
ub = 0;
x = gamultiobj(FitnessFunction,numberOfVariables,A,b,Aeq,beq,lb,ub);
% All solutions in X (each row) will satisfy all linear and bound
% constraints within the tolerance specified in options.TolCon. However, if
% you use your own crossover or mutation function, ensure that the new
% individuals are feasible with respect to linear and simple bound
% constraints.
%% Adding Visualization
% |gamultiobj| can accept one or more plot functions through the options
% argument. This feature is useful for visualizing the performance of the
% solver at run time. Plot functions can be selected using |gaoptimset|. The
% help for |gaoptimset| contains a list of plot functions to choose from.
% Here we use |gaoptimset| to create an options structure to select two plot
```

```
% functions. The first plot function is GAPLOTPARETO, which plots the
% Pareto front (limited to any three objectives) at every generation. The
% second plot function is GAPLOTSCOREDIVERSITY, which plots the score
% diversity for each objective. The options structure is passed as the last
% argument to the solver.
options = gaoptimset('PlotFcns',{@gaplotpareto,@gaplotscorediversity});
gamultiobj(FitnessFunction,numberOfVariables,[],[],[],[],lb,ub,options);
%% Vectorizing Your Fitness Function
% Consider the previous fitness functions again:
%
%     objective1(x) = (x+2)^2 - 10, and
%     objective2(x) = (x-2)^2 + 20
%
% By default, the |gamultiobj| solver only passes in one point at a time to the
% fitness function. However, if the fitness function is vectorized to
% accept a set of points and returns a set of function values you can speed
% up your solution.
%
% For example, if the solver needs to evaluate five points in one call to
% this fitness function, then it will call the function with a matrix of
% size 5-by-1, i.e., 5 rows and 1 column (recall that 1 is the number of
% variables).
%
% Create a MATLAB-file called vectorized_multiobjective.m:
%
%     function scores = vectorized_multiobjective(pop)
%       popSize = size(pop,1); % Population size
%       numObj = 2;  % Number of objectives
%       % initialize scores
%       scores = zeros(popSize, numObj);
%       % Compute first objective
%       scores(:,1) = (pop + 2).^2 - 10;
%       % Compute second obective
%       scores(:,2) = (pop - 2).^2 + 20;
%
% This vectorized version of the fitness function takes a matrix 'pop' with
% an arbitrary number of points, the rows of 'pop', and returns a matrix of
% size populationSize-by-numberOfObjectives.
%
% We need to specify that the fitness function is vectorized using the
% options structure created using |gaoptimset|. The options structure is
% passed in as the ninth argument.

FitnessFunction = @(x) vectorized_multiobjective(x);
options = gaoptimset('Vectorized','on');
gamultiobj(FitnessFunction,numberOfVariables,[],[],[],[],lb,ub,options);

displayEndOfDemoMessage(mfilename)
```

`

Appendix C: Simple Multiobjective Function

```
function y = Network_multiobjective(x)
%SIMPLE_MULTIOBJECTIVE is a simple multi-objective fitness function.
%
% The multi-objective genetic algorithm solver assumes the fitness function
% will take one input x where x is a row vector with as many elements as
% number of variables in the problem. The fitness function computes the
% value of each objective function and returns the vector value in its one
% return argument y.

%   Copyright 2007 The MathWorks, Inc.

% Spindle Speeds
input(1,1)= 500;
input(1,2)= 710;
input(1,3)= 1000;
input(1,4)= 1400;

%Feed Rates
input(2,1)= 63;
input(2,2)= 100;
input(2,3)= 160;
input(2,4)= 250;

% Elongation
S(1,1)= 9.86;
S(1,3)= 12.58;
S(1,4)= 9.22;
S(2,4)= 10.17;
S(3,1)= 11.15;
S(3,3)= 7.21;
S(4,1)= 6.83;
S(4,2)= 5.95;

%Ultimate Strength
S1(1,1)= 408.52589;
S1(1,3)= 501.4152072;
S1(1,4)= 483.3609847;
S1(2,4)= 498.5870329;
S1(3,1)= 405.223754;
S1(3,3)= 408.0955743;
S1(4,1)= 375.1482436;
S1(4,2)= 350.9981734;

%Hardness
S2(1,1)= 118.92;
S2(1,3)= 136.32;
S2(1,4)= 154.775;
S2(2,4)= 153.8556;
```

```
`


S2(3,1)= 117.0111;
S2(3,3)= 141.2286;
S2(4,1)= 132.5875;
S2(4,2)= 128.8143;

%Power Consumption

S3(1,1)= 0.338005656;
S3(1,3)= 0.164229395;
S3(1,4)= 0.115391948;
S3(2,4)= 0.122219246;
S3(3,1)= 0.34822381;
S3(3,3)= 0.161734978;
S3(4,1)= 0.359842893;
S3(4,2)= 0.247245174;

input1=input(1,1:end);
input2=input(2,1:end);

% Draw the initial data from Experiments
subplot(4,2,1);
surf(input1,input2,S,'FaceColor','interp','EdgeColor','none','FaceLighting','phong');
title('Elongation-original');
axis tight
view(-50,30)
camlight right

subplot(4,2,3);
surf(input1,input2,S1,'FaceColor','interp','EdgeColor','none','FaceLighting','phong');
title('Ultimate Stregth-original');
axis tight
view(-50,30)
camlight right

subplot(4,2,5);
surf(input1,input2,S2,'FaceColor','interp','EdgeColor','none','FaceLighting','phong');
title('Hardness-original');
axis tight
view(-50,30)
camlight right

subplot(4,2,7);
surf(input1,input2,S3,'FaceColor','interp','EdgeColor','none','FaceLighting','phong');
title('Powr Consumption-original');
axis tight
view(-50,30)
camlight right

%-----Feedforward Backpropogation Neural Networks Algorithm------
%-----creating a neural network and training it----------
```

`

```
I=[input1;input2];
net = feedforwardnet;
net.trainParam.epochs =5;
net.trainParam.lr= 0.01;
net.numLayers = 3;
net.layers{1}.size = 50;
net.layers{2}.size = 50;
net.layers{3}.size = 50;
%net.layers{4}.size = 35;

net.biases{1}.learnFcn = 'learnp';
net = configure(net,I,S);

net=train(net,I,S);
%view(net);
z=net(I);
perf=perform(net,z,S);

dx1=1;
dy1=1;

x1_edge=[floor(min(input1)):dx1:ceil(max(input1))];
y1_edge=[floor(min(input2)):dy1:ceil(max(input2))];
[X1,Y1]=meshgrid(x1_edge,y1_edge);
Z=griddata(input1,input2,z,X1,Y1);

subplot(4,2,2);

surf(X1,Y1,Z,'FaceColor','interp','EdgeColor','none','FaceLighting','phong');
%surf(input1,input2,z,'FaceColor','interp','EdgeColor','none','FaceLighting','phong');
title('Elongation-NN');
%daspect([5 5 1])
axis tight
view(-50,30)
camlight left

%camlight left; lighting phong;
A=max(max(S));%minimum value of the shubert function
%A=min(min(Z));%minimum value of the approximated initial function
B=max(max(Z));%minimum value of the created network
errors = gsubtract(A,B);

%Train the Ultimate Stength
net1 = configure(net,I,S1);

net1=train(net1,I,S1);
%view(net);
z1=net1(I);
perf1=perform(net1,z1,S1);
```

```
`


dx1=1;
dy1=1;

x1_edge=[floor(min(input1)):dx1:ceil(max(input1))];
y1_edge=[floor(min(input2)):dy1:ceil(max(input2))];
[X1,Y1]=meshgrid(x1_edge,y1_edge);
Z1=griddata(input1,input2,z1,X1,Y1);

subplot(4,2,4);

surf(X1,Y1,Z1,'FaceColor','interp','EdgeColor','none','FaceLighting','phong');
%surf(input1,input2,z1,'FaceColor','interp','EdgeColor','none','FaceLighting','phong');
title('Ultimate Stregth-NN');
%daspect([5 5 1])
axis tight
view(-50,30)
camlight left

%camlight left; lighting phong;
A1=min(min(S1));%minimum value of the shubert function
%A=min(min(Z));%minimum value of the approximated initial function
B1=min(min(Z1));%minimum value of the created network
errors1 = gsubtract(A1,B1);

%Train the Hardness
net2 = configure(net,I,S2);

net2=train(net2,I,S2);
%view(net);
z2=net2(I);
perf2=perform(net2,z2,S2);

dx1=1;
dy1=1;

x1_edge=[floor(min(input1)):dx1:ceil(max(input1))];
y1_edge=[floor(min(input2)):dy1:ceil(max(input2))];
[X1,Y1]=meshgrid(x1_edge,y1_edge);
Z2=griddata(input1,input2,z2,X1,Y1);

subplot(4,2,6);

surf(X1,Y1,Z2,'FaceColor','interp','EdgeColor','none','FaceLighting','phong');
%surf(input1,input2,z2,'FaceColor','interp','EdgeColor','none','FaceLighting','phong');
title('Hardness-NN');
%daspect([5 5 1])
axis tight
view(-50,30)
camlight left
```

`

```
%camlight left; lighting phong;
A2=min(min(S2));%minimum value of the shubert function
%A=min(min(Z));%minimum value of the approximated initial function
B2=min(min(Z2));%minimum value of the created network
errors2 = gsubtract(A2,B2);

%Train the Cost of Energy
net3 = configure(net,I,S3);

net3=train(net3,I,S3);
%view(net);
z3=net3(I);
perf3=perform(net3,z3,S3);

dx1=1;
dy1=1;

x1_edge=[floor(min(input1)):dx1:ceil(max(input1))];
y1_edge=[floor(min(input2)):dy1:ceil(max(input2))];
[X1,Y1]=meshgrid(x1_edge,y1_edge);
Z3=griddata(input1,input2,z3,X1,Y1);

subplot(4,2,8);

surf(X1,Y1,Z3,'FaceColor','interp','EdgeColor','none','FaceLighting','phong');
%surf(input1,input2,z3,'FaceColor','interp','EdgeColor','none','FaceLighting','phong');
title('Power Consumption-NN');
%daspect([5 5 1])
axis tight
view(-50,30)
camlight left

%camlight left; lighting phong;
A3=min(min(S3));%minimum value of the shubert function
%A=min(min(Z));%minimum value of the approximated initial function
B3=min(min(Z3));%minimum value of the created network
errors3 = gsubtract(A3,B3);

XX = round(x(1));
YY = round(x(2));

if XX >= 63
   II=XX-63;
else
   II=1;
end

if XX >= 250
   II=188;
end
```

`

```
if YY >= 500
   JJ=YY-500;
else
    JJ=1;
end

if YY > 1400
    JJ=901;
end

y(1)=Z(II,JJ);

y(2)=Z1(II,JJ);

y(3)=Z2(II,JJ);

y(4)=Z3(II,JJ);
```

`

Appendix D: Shubert Function

```
%shubert function
clc
clear all

% Performing a Multiobjective Optimization Using the Genetic Algorithm
% This example shows how to perform a multiobjective optimization
% using multiobjective genetic algorithm function |gamultiobj| in
% Global Optimization Toolbox.

%   Copyright 2007-2012 The MathWorks, Inc.

% Simple Multiobjective Optimization Problem
% |gamultiobj| can be used to solve multiobjective optimization problem in
% several variables. Here we want to minimize two objectives, each having
% one decision variable.
%
%     min F(x) = [objective1(x); objective2(x)]
%      x
%
%     where, objective1(x) = (x+2)^2 - 10, and
%           objective2(x) = (x-2)^2 + 20

% Plot two objective functions on the same axis
%
% The two objectives have their minima at x = -2 and x = +2 respectively.
% However, in a multiobjective problem, x = -2, x = 2, and any solution in
% the range -2 <= x <= 2 is equally optimal. There is no single solution to
% this multiobjective problem. The goal of the multiobjective genetic
% algorithm is to find a set of solutions in that range (ideally with a
% good spread). The set of solutions is also known as a Pareto front. All
% solutions on the Pareto front are optimal.

%%  Coding the Fitness Function
% We create a MATLAB-file named simple_multiobjective.m:
%
%     function y = simple_multiobjective(x)
%     y(1) = (x+2)^2 - 10;
%     y(2) = (x-2)^2 + 20;
%
% The Genetic Algorithm solver assumes the fitness function will take one
% input x, where x is a row vector with as many elements as the number of
% variables in the problem. The fitness function computes the value of
% each objective function and returns these values in a single vector
% output y.

%% Minimizing Using |gamultiobj|
% To use the |gamultiobj| function, we need to provide at least two input
% arguments, a fitness function, and the number of variables in the problem.
```

```
% The first two output arguments returned by |gamultiobj| are X, the points
% on Pareto front, and FVAL, the objective function values at the values X.
% A third output argument, exitFlag, tells you the reason why |gamultiobj|
% stopped. A fourth argument, OUTPUT, contains information about the
% performance of the solver. |gamultiobj| can also return a fifth argument,
% POPULATION, that contains the population when |gamultiobj| terminated and a
% sixth argument, SCORE, that contains the function values of all
% objectives for POPULATION when |gamultiobj| terminated.
FitnessFunction = @mostafa_multiobjective;
numberOfVariables = 2;
%[x,fval] = gamultiobj(FitnessFunction,numberOfVariables);

% The X returned by the solver is a matrix in which each row is the
% point on the Pareto front for the objective functions. The FVAL is a
% matrix in which each row contains the value of the objective functions
% evaluated at the corresponding point in X.
%size(x)
%size(fval)

%% Constrained Multiobjective Optimization Problem
% |gamultiobj| can handle optimization problems with linear inequality,
% equality, and simple bound constraints. Here we want to add bound
% constraints on simple multiobjective problem solved previously.
%
%    min F(x) = [objective1(x); objective2(x)]
%     x
%    subject to  -1.5 <= x <= 0 (bound constraints)
%
%    where, objective1(x) = (x+2)^2 - 10, and
%           objective2(x) = (x-2)^2 + 20

% |gamultiobj| accepts linear inequality constraints in the form A*x <= b and
% linear equality constraints in the form Aeq*x = beq and bound constraints
% in the form lb < x < ub. We pass A and Aeq as matrices and b, beq, lb,
% and ub as vectors. Since we have no linear constraints in this example, we
% pass [] for those inputs.
A = []; b = [];
Aeq = []; beq = [];
lb = [500 63]; % Lower bound
ub = [1400 250]; % Upper bound
%options = gaoptimset('PlotFcns',@gaplotpareto);
x = gamultiobj(FitnessFunction,numberOfVariables,A,b,Aeq,beq,lb,ub);

% All solutions in X (each row) will satisfy all linear and bound
% constraints within the tolerance specified in options.TolCon. However, if
% you use your own crossover or mutation function, ensure that the new
% individuals are feasible with respect to linear and simple bound
% constraints.

%% Adding Visualization
```

```
% |gamultiobj| can accept one or more plot functions through the options
% argument. This feature is useful for visualizing the performance of the
% solver at run time. Plot functions can be selected using |gaoptimset|. The
% help for |gaoptimset| contains a list of plot functions to choose from.
%
% Here we use |gaoptimset| to create an options structure to select two plot
% functions. The first plot function is GAPLOTPARETO, which plots the
% Pareto front (limited to any three objectives) at every generation. The
% second plot function is GAPLOTSCOREDIVERSITY, which plots the score
% diversity for each objective. The options structure is passed as the last
% argument to the solver.
options = gaoptimset('PlotFcns',{@gaplotpareto,@gaplotscorediversity});
gamultiobj(FitnessFunction,numberOfVariables,[],[],[],[],lb,ub,options);

%% Vectorizing Your Fitness Function
% Consider the previous fitness functions again:
%
%     objective1(x) = (x+2)^2 - 10, and
%     objective2(x) = (x-2)^2 + 20
%
% By default, the |gamultiobj| solver only passes in one point at a time to the
% fitness function. However, if the fitness function is vectorized to
% accept a set of points and returns a set of function values you can speed
% up your solution.
%
% For example, if the solver needs to evaluate five points in one call to
% this fitness function, then it will call the function with a matrix of
% size 5-by-1, i.e., 5 rows and 1 column (recall that 1 is the number of
% variables).
%
% Create a MATLAB-file called vectorized_multiobjective.m:
%
%     function scores = vectorized_multiobjective(pop)
%       popSize = size(pop,1); % Population size
%       numObj = 2;  % Number of objectives
%       % initialize scores
%       scores = zeros(popSize, numObj);
%       % Compute first objective
%       scores(:,1) = (pop + 2).^2 - 10;
%       % Compute second obective
%       scores(:,2) = (pop - 2).^2 + 20;
%
% This vectorized version of the fitness function takes a matrix 'pop' with
% an arbitrary number of points, the rows of 'pop', and returns a matrix of
% size populationSize-by-numberOfObjectives.
%
% We need to specify that the fitness function is vectorized using the
% options structure created using |gaoptimset|. The options structure is
% passed in as the ninth argument.
%displayEndOfDemoMessage(mfilename)
```

`

Appendix E : Multiobjective Fitness Function

```
function y = simple_multiobjective(x)
%SIMPLE_MULTIOBJECTIVE is a simple multi-objective fitness function.
%
% The multi-objective genetic algorithm solver assumes the fitness function
% will take one input x where x is a row vector with as many elements as
% number of variables in the problem. The fitness function computes the
% value of each objective function and returns the vector value in its one
% return argument y.

%   Copyright 2007 The MathWorks, Inc.

y(1) = (x+2)^2 - 10;
y(2) = (x-2)^2 + 20;
```